Glassy correlations and microstructures in randomly cross-linked homopolymer blends

Christian Wald[a)]
Institut für Theoretische Physik, Georg-August-Universität Göttingen, Friedrich-Hund-Platz 1, 37077 Göttingen

Paul M. Goldbart
Department of Physics, University of Illinois at Urbana-Champaign, Urbana, Illinois 61806-3080

Annette Zippelius[b)]
Institut für Theoretische Physik, Georg-August-Universität Göttingen, Friedrich-Hund-Platz 1, 37077 Göttingen

(Received 27 September 2005; accepted 6 April 2006; published online 6 June 2006)

We consider a microscopic model of a polymer blend that is prone to phase separation. Permanent cross-links are introduced between randomly chosen pairs of monomers, drawn from the Deam-Edwards distribution. Thereby, not only density but also concentration fluctuations of the melt are quenched-in in the gel state, which emerge upon sufficient cross-linking. We derive a Landau expansion in terms of the order parameters for gelation and phase separation, and analyze it on the mean-field level, including Gaussian fluctuations. The mixed gel is characterized by thermal as well as time-persistent (glassy) concentration fluctuations. Whereas the former are independent of the preparation state, the latter reflect the concentration fluctuations at the instant of cross-linking, provided the mesh size is smaller than the correlation length of phase separation. The mixed gel becomes unstable to microphase separation upon lowering the temperature in the gel phase. Whereas the length scale of microphase separation is given by the mesh size, at least close to the transition, the emergent microstructure depends on the composition and compressibility of the melt. Hexagonal structures, as well as lamellas or random structures with a unique wavelength, can be energetically favorable. © *2006 American Institute of Physics*. [DOI: 10.1063/1.2200697]

I. INTRODUCTION

Cross-linked homopolymer blends exhibit a rich phase diagram due to the competition between phase separation and cross-linking. The simplest case is a blend of two homopolymer species, A and B, whose incompatibility is controlled by the Flory-Huggins parameter χ and which are cross-linked irreversibly by some number N_c of chemical bonds. In addition, the concentration fluctuations can be controlled independently in the process of cross-linking (preparation state) and the well cross-linked gel (measurement state), e.g., by lowering the temperature in the gel. Hence we have three control parameters: the incompatibility χ_p in the preparation state, the incompatibility χ_m in the measurement state, and the number of cross-links per chain, $\mu=N_c/N$, where N denotes the total number of chains in the melt.

A statistical mechanical theory thus has to include not only the average over the quenched disorder (cross-link realization) but also the "memory" of the preparation state. This can be achieved in the following way: We start from a microscopic model, which accounts for the repulsive interaction of all monomers, irrespective of species (excluded volume), as well as for a repulsive interaction between the different species only (incompatibility). Cross-links are introduced between randomly chosen pairs of monomers. The probability for a particular cross-link configuration depends on the *preparation state* of the system, such that monomers with a high probability to be close in the preparation state have a high probability to be cross-linked. Thereby the cross-links indeed preserve the memory of the preparation state. Mathematically, this is achieved via the Deam-Edwards distribution[1] and the replica trick to average over the quenched disorder.

We expect and indeed find signatures of the preparation state in the gel. An example is given by the concentration fluctuations that are frozen in by the cross-links. The frustration between the tendency towards phase separation of incompatible macromolecules and the connectivity constraints of the network gives rise to glassy, i.e., time persistent, concentration fluctuations. If the preparation state is close to macroscopic phase separation, then these glassy fluctuations reflect the correlations in the melt at the moment of cross-linking. If, on the other hand, the preparation state is far from phase separation, then the frozen fluctuations are completely random and follow the pattern set by the cross-links.

Lowering the temperature in the gel or, equivalently, increasing the incompatibility at measurement χ_m will ultimately give rise to microphase separation, while macroscopic demixing is suppressed by the cross-links. A variety of microphases can exist, depending on the composition of

[a)]Electronic mail: wald@theorie.physik.uni-goettingen.de
[b)]Electronic mail: annette@theorie.physik.uni-goettingen.de

the blend and its compressibility. If the mixture is symmetric, having equal concentrations of A and B monomers, then lamellas are energetically favorable, whereas for an asymmetric mixture hexagons prevail. A finite compressibility enhances the tendency towards phase separation and can induce a random pattern consisting of a superposition of many lamellar phases of different orientations. In all cases the critical wave number is given by the mesh size or localization length of the gel.

The subject of cross-linked homopolymer blends was first addressed by de Gennes,[2] who pointed out that the mixed state is stabilized in the gel and eventually undergoes microphase separation. His predictions were verified experimentally[3,4] with, however, a discrepancy in the scattering intensity for small wave number. This was traced back to the neglect of concentration fluctuations, which are present during cross-linking and are partially frozen in by the cross-links. Subsequently, several attempts were made to include these effects approximately.[3,5–7] Studies of cross-linked systems, based on the microscopic model by Panyukov and Rabin,[8] were reported by Sfatos and Shakhnovich;[9] as far as homopolymer blends are concerned, these authors recover de Gennes result within a microscopic approach. Computer simulations were carried out by Lay *et al.*[10] who studied, in particular, the relation of the domain sizes to the mesh size of the gel. In the last section of our paper we present a detailed discussion of the literature in comparison with our own results.

The paper is organized as follows: In Sec. II we formulate a microscopic model of cross-linked polymer chains. Subsequently (Sec. III) we derive a Landau expansion in terms of the order parameters for gelation and phase separation. The Landau theory allows us to discuss the mixed gel (Sec. IV) as well as microphase separation (Sec. V). We conclude with a short summary, a comparison with previous theoretical work, and an outlook. A short account of our results for the special case of an incompressible melt with equal concentrations of A and B monomers was given previously in Ref. 11.

II. MODEL

A. Uncross-linked homopolymer blend

We first consider an *uncross-linked* blend of polymer, modeled as a system of Gaussian phantom chains of equal degree of polymerization L and step length b. The melt is taken to contain N_A chains of type A and N_B chains of type B. In general, there will be an imbalance in concentration $q := (N_A - N_B)/N$, where $N = N_A + N_B$ is the total number of chains, occupying a volume $\mathcal{V}$ in d-dimensional space. The monomer positions are denoted as $\boldsymbol{R}_{a,i}(s)$, where $a = A, B$ refers to the chain species, $i = 1, \ldots, N_a$ enumerates the chains, and $s = 0, \ldots, 1$ is the continuous index for a "site"on a chain. It turns out to be convenient to express the monomer positions by dimensionless vectors $\boldsymbol{r}_{a,i}(s) = \sqrt{d/Lb^2}\boldsymbol{R}_{a,i}(s)$, so that all lengths are measured in units of the radius of gyration of the free chains, $R_g^2 = Lb^2/6$. The rescaled volume reads $V := (d/Lb^2)^{d/2}\mathcal{V}$.

The chain connectivity is described by the usual Wiener Hamiltonian

$$H^W = \frac{k_B T}{2} \sum_{a=A,B} \sum_{i=1}^{N_a} \int_0^1 ds \left(\frac{d\boldsymbol{r}_{a,i}(s)}{ds} \right)^2, \tag{1}$$

the excluded volume term controlling compressibility reads

$$H^\lambda = \frac{V k_B T \lambda}{4N} \sum_{a,a'=A,B} \sum_{i,i'=1}^{N_a} \int_0^1 ds \int_0^1 ds' \, \delta(\boldsymbol{r}_{a,i}(s) - \boldsymbol{r}_{a',i'}(s')), \tag{2}$$

and the incompatibility of the two monomer species is modeled by the interaction

$$H^\chi = -\frac{V\chi}{4N} \sum_{a,a'=A,B} (2\delta_{a,a'} - 1) \times \sum_{i,i'=1}^{N_a} \int_0^1 ds \int_0^1 ds' \, \delta(\boldsymbol{r}_{a,i}(s) - \boldsymbol{r}_{a',i'}(s')). \tag{3}$$

Although the chain elasticity and the volume exclusion are of mainly entropic origin, the incompatibility is assumed to be a chiefly energetic contribution. Nevertheless, we let $k_B T = 1$ in the following to simplify the expressions. Instead of changing the temperature, we shall tune λ and particularly χ, which will serve as the inverse temperature.

B. Cross-linking

Chemical cross-linking induces a random number M of permanent bonds between randomly selected pairs of monomers; a particular realization of cross-links is denoted by $\mathcal{C} = \{(a_e, i_e, s_e, a'_e, i'_e, s'_e)\}_{e=1}^M$. The links are modeled as hard constraints with zero bond length. The partition function of the cross-linked melt, relative to a Rouse melt thus reads

$$Z(\mathcal{C}) := \left\langle \prod_{e=1}^{M} \delta(\boldsymbol{r}_{a_e,i_e}(s_e) - \boldsymbol{r}_{a'_e,i'_e}(s'_e)) \exp\{-H^\lambda - H^\chi\} \right\rangle^W := \frac{\int \mathcal{D}\boldsymbol{r}_{a,i}(s) \prod_{e=1}^M \delta(\boldsymbol{r}_{a_e,i_e}(s_e) - \boldsymbol{r}_{a'_e,i'_e}(s'_e)) \exp\{-H^W - H^\lambda - H^\chi\}}{\int \mathcal{D}\boldsymbol{r}_{a,i}(s) \exp\{-H^W\}}. \tag{4}$$

Here we have implicitly defined the expectation value $\langle \ldots \rangle^W$ with respect to the Wiener Hamiltonian of the uncross-linked melt.

C. Disorder average and Deam-Edwards distribution

We are interested in the properties of the "generic" melt rather than in the properties of a melt with a specific set of cross-links. Furthermore, we assume the system to be self-averaging in the thermodynamic limit. Therefore we will consider *disorder averages* of the observables with respect to the quenched randomness of cross-links.

We specify the probability distribution of the cross-link sets following the strategy of Deam and Edwards.[1] We suppose that the dominant cross-link sets are those that are most compatible with the uncross-linked melt. More precisely, we assume a probability distribution

$$\mathbb{P}_M(\mathcal{C}) \propto \frac{(\mu N/V)^M}{M!} Z_p(\mathcal{C}). \tag{5}$$

Here, Z_p is given by Eq. (4), evaluated at $\lambda=\lambda_p$ and $\chi=\chi_p$, which characterize the system prior to cross-linking. Disorder averages with respect to $\mathbb{P}_M$ will be denoted by square brackets.

D. Order parameters for the homopolymer blend

To discriminate between the liquid state and the amorphous solid state of the polymer system, we use the order parameter proposed in Ref. 12 as follows:

$$\tilde{\Omega}_{\boldsymbol{k}_1,\ldots,\boldsymbol{k}_g} := \frac{1}{N} \sum_{a=A,B} \sum_{i=1}^{N_a} \int_0^1 ds \langle \exp(i\boldsymbol{k}_1 \boldsymbol{r}_{a,i}(s)) \rangle_{\mathcal{C}} \times \cdots \times \langle \exp(i\boldsymbol{k}_g \boldsymbol{r}_{a,i}(s)) \rangle_{\mathcal{C}}, \tag{6}$$

for $g=1,2,\ldots$, and nonzero $\{\boldsymbol{k}_\gamma\}$. The symbol $\langle \cdots \rangle_{\mathcal{C}}$ denotes the thermal expectation value in the presence of a particular realization $\mathcal{C}$ of cross-links. In the case $g=1$, Eq. (6) is the thermal average of the monomer density in Fourier space,

$$\tilde{\rho}_{\boldsymbol{k}} := \frac{1}{N} \sum_{a=A,B} \sum_{i=1}^{N_a} \int_0^1 ds e^{-i\boldsymbol{k}\boldsymbol{r}_{a,i}(s)}. \tag{7}$$

In the liquid state, a monomer explores the sample volume uniformly. Hence, the equilibrium value of the local density is constant and the Fourier transform $\langle \exp(i\boldsymbol{k}\boldsymbol{r}_i(s)) \rangle_{\mathcal{C}}$ vanishes (except for $\boldsymbol{k}=\boldsymbol{0}$, which we exclude). The order parameter (6) therefore is always zero in the liquid state.

In a solid, at least a finite fraction of the monomers are localized about points $\boldsymbol{b}_{a,i}(s)$ in space. For these monomers, $\langle \exp(i\boldsymbol{k}\boldsymbol{r}_{a,i}(s)) \rangle_{\mathcal{C}} \propto e^{i\boldsymbol{k}\boldsymbol{b}_{a,i}(s)} \neq 0$. However, for an amorphous, i.e., macroscopically translationally invariant (MTI) solid, the disorder averaged expectation value $[\tilde{\Omega}_{\boldsymbol{k}_1,\ldots,\boldsymbol{k}_g}]$ vanishes unless $\boldsymbol{k}_1+\cdots+\boldsymbol{k}_g=0$, see Ref. 12. In particular, $[\langle \tilde{\rho}_{\boldsymbol{k}} \rangle_{\mathcal{C}}]=0$ in the MTI state. Hence we can discriminate between the liquid and the amorphous solid states by means of the $g \geqslant 2$ values of Eq. (6). (For the signature of crystalline and globular states, see Ref. 12).

Throughout this article, we will also refer to the two monomer species as "opposite charges." The identification of As and Bs with positive and negative charges, respectively, leads to a natural choice for an order parameter detecting phase separation: the "charge density"

$$\tilde{\Psi}_{\boldsymbol{k}} := \frac{1}{N} \sum_{i=1}^{N_A} \int_0^1 ds e^{-i\boldsymbol{k}\boldsymbol{r}_{A,i}(s)} - \frac{1}{N} \sum_{i=1}^{N_B} \int_0^1 ds e^{-i\boldsymbol{k}\boldsymbol{r}_{B,i}(s)} \tag{8}$$

measuring the local imbalance of the concentrations of A and B.

In the general case of an asymmetric blend, in which there is an excess of either A or B chains, the average charge density is given by $q \cdot N/V=(N_A-N_B)/V$, so that $\tilde{\Psi}_{\boldsymbol{k}}$ serves as an order parameter only for $\boldsymbol{k} \neq 0$. Homogeneous phase separation is indicated by a nonzero expectation value of the order parameter in the limit $k \to 0$. Microstructures, e.g., lamellas or hexagonally ordered cylinders, give rise to a nonzero expectation value of $[\langle \tilde{\Psi}_{\boldsymbol{k}} \rangle_{\mathcal{C}}]$ at finite wave number. A nonuniform charge density, in general, is accompanied by mass density modulations, except for the incompressible case.

In the gel phase we expect to find static charge fluctuations $\langle \tilde{\Psi}_{\boldsymbol{k}} \rangle_{\mathcal{C}} \neq 0$ for all wave numbers. If the gel state is a homogeneous mixture of A and B chains, then the disorder averaged charge density vanishes, i.e., $[\langle \tilde{\Psi}_{\boldsymbol{k}} \rangle_{\mathcal{C}}]=0$. The frozen-in fluctuations can only be detected by the glassy correlations $[\langle \tilde{\Psi}_{\boldsymbol{k}} \rangle_{\mathcal{C}} \langle \tilde{\Psi}_{-\boldsymbol{k}} \rangle_{\mathcal{C}}]$. In general, the quadratic expectation values $[\langle \tilde{\Psi}_{\boldsymbol{k}} \tilde{\Psi}_{-\boldsymbol{k}} \rangle_{\mathcal{C}}]$ and $[\langle \tilde{\Psi}_{\boldsymbol{k}} \rangle_{\mathcal{C}} \langle \tilde{\Psi}_{-\boldsymbol{k}} \rangle_{\mathcal{C}}]$ measure volatile and time-persistent charge fluctuations in an *a priori* homogeneous mixture.

III. EFFECTIVE FREE ENERGY

The disorder averaged free energy

$$F = -[\ln Z(\mathcal{C})] = -\lim_{n \to 0} \frac{[(Z)^n]-1}{n} \tag{9}$$

is computed with the help of the replica trick. The nth power of Z is made explicit using n independent copies (*replicas*) of the system and an additional replica is introduced to account for the Deam-Edwards distribution.[12] The average over the disorder can be carried out explicitly, yet at the cost of a coupling between the formerly independent replicas, yielding

$$[Z^n] =: \mathcal{Z}_n/\mathcal{Z}_0, \tag{10}$$

where the replicated partition function is given by

$$\mathcal{Z}_n = \left\langle \exp\left\{ -H^{\lambda}_{n+1} - H^{\chi}_{n+1} + \frac{\mu V}{4N} \sum_{a,a'=A,B} \sum_{i,i'=1}^{N} \int_0^1 ds ds' \prod_{\alpha=0}^{n} \delta(\boldsymbol{r}^{\alpha}_{a,i}(s) - \boldsymbol{r}^{\alpha}_{a',i'}(s')) \right\} \right\rangle^{W}_{n+1}. \tag{11}$$

Here, the $\boldsymbol{r}^{\alpha}_{a,i}(s)$ denotes the monomer positions in the αth replica, $\langle \cdots \rangle^{W}_{n+1}$ is the replicated Wiener average, and H^{λ}_{n+1} and H^{χ}_{n+1} denote the replicated Hamiltonians of the excluded volume and incompatibility interactions. The denominator and the zeroth replica in the numerator are due to the Deam-Edwards distribution (5) and reflect the situation *prior* to cross-linking. Thus, we have to distinguish between the zeroth replica, characterized by λ_p and χ_p (*preparation ensemble*), and the other n replicas, reflecting the situation *after cross-linking*, characterized by λ_m and χ_m (*measurement ensemble*). To account for the particular role of the zeroth replica we use the notation

$$\lambda^{\alpha} := \begin{cases} \lambda_p & \text{if } \alpha = 0 \\ \lambda_m & \text{otherwise} \end{cases}$$

and

$$\chi^{\alpha} := \begin{cases} \chi_p & \text{if } \alpha = 0 \\ \chi_m & \text{otherwise.} \end{cases} \tag{12}$$

The many-particle problem of the polymer melt can be formally reduced to a two-chain problem (one chain of each species). It is convenient to introduce $(n+1)$-fold replicated vectors $\hat{x} := (\boldsymbol{x}^0, \ldots, \boldsymbol{x}^n)$, and to express the exponents in Eq. (11) in Fourier space, which leads to quadratic terms in the monomer and charge densities. These can be linearized by means of Hubbard-Stratonovich transformations, yielding

$$\mathcal{Z}_n = \mathcal{B}_n \cdot \int \mathcal{D}(\{\Psi, \Omega, \rho\}) \exp\{-n\mathcal{F}_n(\{\Psi, \Omega, \rho\})\} \tag{13}$$

with a constant $\mathcal{B}_n = \exp\{(N/2)(-n\lambda_m + nq^2\chi_m + ((n+1)V^{-n} - 1)\mu)\} = 1 + \mathcal{O}(n)$ and the *effective free energy*

$$n\mathcal{F}_n(\{\Psi, \Omega\rho\}) = \frac{N}{2} {\sum_{\alpha,\boldsymbol{k}}}' \left(\left(\frac{1}{\chi^{\alpha}} - \frac{q^2}{\tilde{\lambda}^{\alpha}} \right) |\Psi^{\alpha}_{\boldsymbol{k}}|^2 + \frac{1}{\tilde{\lambda}^{\alpha}} |\rho^{\alpha}_{\boldsymbol{k}}|^2 + \frac{iq}{\tilde{\lambda}^{\alpha}} (\rho^{\alpha}_{\boldsymbol{k}} \Psi^{\alpha}_{-\boldsymbol{k}} + \rho^{\alpha}_{-\boldsymbol{k}} \Psi^{\alpha}_{\boldsymbol{k}}) \right)$$
$$+ \frac{NV^n}{2\mu} \overline{\sum_{\hat{k}}} |\Omega_{\hat{k}}|^2 - N_A \ln z_+(\{\Psi, \Omega, \rho\}) - N_B \ln z_-(\{\Psi, \Omega, \rho\}), \tag{14}$$

where

$$z_{\pm}(\{\Psi, \Omega, \rho\}) := \left\langle \exp\left\{ {\sum_{\alpha,\boldsymbol{k}}}' (+i\rho^{\alpha}_{\boldsymbol{k}} - (q \mp 1)\Psi^{\alpha}_{\boldsymbol{k}}) \int_0^1 ds e^{i\boldsymbol{k}\mathbf{r}^{\alpha}(s)} + V^{-n} \overline{\sum_{\hat{k}}} \Omega_{\hat{k}} \cdot \int_0^1 ds e^{i\hat{k}\hat{r}(s)} \right\} \right\rangle^{W}_{n+1}. \tag{15}$$

The Wiener average now runs over a *single replicated chain* having monomer positions $\hat{r}(s)$. The auxiliary fields $\Psi_{\boldsymbol{k}}$, $\rho_{\boldsymbol{k}}$, and $\Omega_{\hat{k}}$ are pairwise dependent via $\Omega_{-\hat{k}} = (\Omega_{\hat{k}})^*$, etc., thus the Ψ and Ω integrations in (13) are restricted to the half-spaces $\boldsymbol{k} \cdot \boldsymbol{n} > 0$ and $\hat{k} \cdot \hat{n} > 0$ (with arbitrary nonzero constants $\boldsymbol{n}$ and $\hat{n}$). The sums over the $\boldsymbol{k}^{\alpha}$ and $\hat{k}$ are split into *replica sectors*: The constant part $\mathcal{B}_n$ is composed of the $\boldsymbol{k}^{\alpha} = \boldsymbol{0}$ and $\hat{k} = \hat{0}$ contributions (*zero replica sector*). The symbols $\Sigma'_{\boldsymbol{k}}$ and $\overline{\Sigma}'_{\hat{k}}$ denote the sums over nonzero $\boldsymbol{k}$ (*single replica sector*) and over $\hat{k}$ with nonzero $\boldsymbol{k}^{\alpha}$ in at least two replicas (*higher replica sector*), respectively, both restricted to the above subspaces.

As expected, cross-links give rise to an attractive interaction between the chains, which, in the absence of excluded volume, would cause the chains to collapse into a globular state. A sufficiently strong excluded volume interaction prevents this collapse, as can be read off the coefficient $\tilde{\lambda}^{\alpha} := \lambda^{\alpha} - \mu/V^n$ of the term quadratic in the density. Stability requires $\lambda_p > \mu$ and $\lambda_m > \mu$.

The physical observables, moments of the local density and charge density, are related to expectation values of the fields according to

$$[\langle \tilde{\Psi}_{\boldsymbol{k}} \rangle_{\mathcal{C}}] = \frac{1}{\chi_m} \lim_{n \to 0} \langle \Psi^{\alpha}_{\boldsymbol{k}} \rangle^{\mathcal{F}}_{n+1} \quad \text{and}$$

$$[\langle \tilde{\rho}_{\boldsymbol{k}} \rangle_{\mathcal{C}}] = \frac{i}{\lambda_m - \mu} \lim_{n \to 0} \langle \rho^{\alpha}_{\boldsymbol{k}} + iq\Psi^{\alpha}_{\boldsymbol{k}} \rangle^{\mathcal{F}}_{n+1}$$

for $\boldsymbol{k} \neq \boldsymbol{0}$ and $\alpha \geqslant \boldsymbol{1}$, and

$$[\tilde{\Omega}_{\boldsymbol{k}_1,\ldots,\boldsymbol{k}_g}] = \frac{1}{\mu}\lim_{n\to 0}\langle\Omega_{\hat{k}}\rangle_{n+1}^{\mathcal{F}}$$

for $\hat{k}=(\mathbf{0},\boldsymbol{k}_1,\ldots,\boldsymbol{k}_g,\mathbf{0},\ldots,\mathbf{0})$ with $g\geqslant 2$.

In asymmetric blends, which have an excess of either A or B chain, the average charge density $qN/V=(N_A-N_B)/V$ is nonzero. To simplify the Landau expansion of the free energy it is then advantageous to either work with the fluctuations $\delta\Psi=\Psi-q$ of the charge density around its mean value or, alternatively, shift the monomer density, as is done here.

IV. HOMOGENEOUSLY MIXED STATES

On the mean-field level, we approximate the functional integral over Ω, ρ, and Ψ in (13) by using the saddle point method, i.e., by the value of the integrand at the point $(\bar{\Psi},\bar{\rho},\bar{\Omega})$ making the integrand stationary:

$$\mathcal{Z}_n \sim \text{const}\cdot e^{-\mathcal{F}_n(\bar{\Psi},\bar{\rho},\bar{\Omega})}, \tag{16}$$

where, by definition, $(\bar{\Psi},\bar{\rho},\bar{\Omega})$ satisfy the stationarity conditions

$$\left.\frac{\partial\mathcal{F}_n}{\partial\Psi_{\boldsymbol{k}}^{\alpha}}\right|_{\bar{\Psi},\bar{\rho},\bar{\Omega}}=0,\qquad \left.\frac{\partial\mathcal{F}_n}{\partial\rho_{\boldsymbol{k}}^{\alpha}}\right|_{\bar{\Psi},\bar{\rho},\bar{\Omega}}=0,\qquad \left.\frac{\partial\mathcal{F}_n}{\partial\Omega_{\hat{k}}}\right|_{\bar{\Psi},\bar{\rho},\bar{\Omega}}=0. \tag{17}$$

A. Homogeneously mixed liquid state

One solution of the stationarity conditions (17) is the trivial saddle point $\bar{\Psi}=\bar{\rho}=\bar{\Omega}=0$, corresponding to the homogeneously mixed liquid state. To assess its stability we consider the Landau expansion to leading order around this point as follows:

$$\begin{aligned}\frac{2n}{\Omega}\mathcal{F}_n(\{\Psi,\rho,\Omega\}) &= \sum_{\alpha,\boldsymbol{k}}{}'\left(\frac{1}{\lambda^n}+g_D(\boldsymbol{k}^2)\right)|\rho_{\boldsymbol{k}}^{\alpha}|^2\\ &+\overline{\sum_{\hat{k}}}\left(\frac{1}{\mu}-g_D(\hat{k}^2)\right)|\Omega_{\hat{k}}|^2+2iq\sum_{\alpha,\boldsymbol{k}}{}'\frac{1}{\lambda^{\alpha}}\Omega_{-\boldsymbol{k}}^{\alpha}\Psi_{\boldsymbol{k}}^{\alpha}\\ &+\sum_{\alpha,\boldsymbol{k}}{}'\left(\frac{1}{\chi^{\alpha}}-\frac{q^2}{\lambda^{\alpha}}-(1-q^2)g_D(\boldsymbol{k}^2)\right)|\Psi_{\boldsymbol{k}}^{\alpha}|^2\\ &+\mathcal{O}(\Psi^2,\rho^2,\Omega^2),\end{aligned} \tag{18}$$

where the Debye function g_D is defined in Appendix B 1. The stability limits of the homogeneous liquid can be read off from the quadratic coefficients. As $g_D(k^2)$ decreases monotonically from 1 to zero, the stability against solidification and demixing require $\mu<1$ and $(\chi_p,\chi_m)<1/(1-q^2)$, respectively. Throughout this article, we assume that $(\lambda_p,\lambda_m)>\mu$, i.e., that the excluded volume interaction is strong enough to prevent density instabilities (see above).

It should be noted that the condition $(\chi_p,\chi_m)<1/(1-q^2)$ denotes local stability *limits* only. In mean-field theory, the phase separation transition for symmetric blends is of second order, so the phase transition coincides with the limit of local stability. In asymmetric blends the transition is of first order. The loss of local stability, as given by the conditions above, then defines a spinodal, and the transition occurs at a lower value of χ. The location of the spinodal depends on the average charge q, with a larger critical incompatibility (i.e., lower critical temperature) for more asymmetric mixtures.

The gelation of the homogeneous liquid, driven by increasing the cross-link concentration, and the microphase separation of the resulting gel, induced by cooling, will be addressed in the following sections.

B. Cross-linking in the homogeneously mixed state

In the liquid state, the polymer blend phase separates macroscopically beyond the demixing threshold. The subsequent gelation of such a macrophase-separated melt would result, apart from the interface, in just two pieces of gels having different compositions. It is more interesting to consider a gel prepared from a homogeneous melt to study phase separation in the gel phase. As we shall see below, such a gel shows glassy charge density patterns and, as anticipated, microphase separation instead of macroscopic demixing. Therefore, the discussion will be restricted to cross-linking in a homogeneously mixed blend, $\chi_p<1/(1-q^2)$, including undercooled mixtures for $q\neq 0$.

Upon gelation, the saddle point $\bar{\Omega}_{\hat{k}}=0$ will become unstable, making it necessary to complement the expansion (18) of the free energy with the third-order terms as follows:

$$\begin{aligned}\frac{2n}{N}\mathcal{F}_n(\{\Psi,\rho,\Omega\}) &= \sum_{\alpha,\boldsymbol{k}}{}'\left(\frac{1}{\chi^{\alpha}}-(1-q^2)g_D(\boldsymbol{k}^2)\right)|\Psi_{\boldsymbol{k}}^{\alpha}|^2\\ &+\overline{\sum_{\hat{k}}}\left(\frac{1}{\mu}-g_D(\hat{k}^2)\right)|\Omega_{\hat{k}}|^2\\ &-\sum_{\alpha_1\neq\alpha_2}\sum_{\boldsymbol{k}_1,\boldsymbol{k}_2}{}'\overline{\sum_{\hat{p}}}\Omega_{\hat{p}}\Psi_{\boldsymbol{k}_1}^{\alpha_1}\Psi_{\boldsymbol{k}_2}^{\alpha_2}\delta_{\boldsymbol{p}^{\alpha_1},\boldsymbol{k}_1}\delta_{\boldsymbol{p}^{\alpha_2}\boldsymbol{k}_2}\\ &-\frac{1}{3}\overline{\sum_{\hat{k}_{1,2,3}}}\Omega_{\hat{k}_1}\Omega_{\hat{k}_2}\Omega_{\hat{k}_3}\delta_{\hat{k}_1+\hat{k}_2+\hat{k}_3\hat{0}},\end{aligned} \tag{19}$$

The vertex functions of the cubic terms have been approximated by their zero wave-number values, the complete expressions being given in Appendix B 1. This approximation is well justified, because the gelation transition is always continuous, so that the relevant length scales are very large, compared with the scales of the microscopic correlations. Here, we have taken the limit of an incompressible melt, which is achieved by integrating out the density fluctuations on the Gaussian level and subsequently taking the limit $\tilde{\lambda}\to\infty$.

We first discuss a gel in the homogeneously mixed state $\bar{\Psi}_{\boldsymbol{k}}^{\alpha}=0$, assuming $\chi_m<1/(1-q^2)$. In the following,[12] we consider the order parameter hypothesis

$$\bar{\Omega}_{\hat{k}}=\delta_{\tilde{\boldsymbol{k}},\mathbf{0}}\cdot Q\int_0^{\infty}d\tau p(\tau)\exp\left(\frac{-\hat{\boldsymbol{k}}^2}{2\tau}\right) \tag{20}$$

with the shorthand $\tilde{\boldsymbol{k}}:=\Sigma_{\alpha=0}^{n}\boldsymbol{k}^{\alpha}$. Here, Q denotes the fraction

of chains that are localized, i.e., the *gel fraction*; the localization lengths are distributed according to the distribution function $p(\tau)$. Both have to be determined self-consistently as a solution of the stationarity conditions (17).

The first two of the stationarity conditions are satisfied for any Q and $p(\tau)$. The third condition is independent of the incompatibility parameter. Hence, in the homogeneously mixed regime, the task of determining Q and $p(\tau)$ on the saddle point level is exactly the same as in the pure gelation problem in Ref. 12. In the present notation, the result for the solid state, i.e., $\mu > 1$, reads

$$\bar{\Omega}_{\hat{k}} \approx \delta_{\tilde{\boldsymbol{k}},\mathbf{0}} \cdot 2\mu(\mu-1) \cdot \omega\left(\sqrt{\frac{4}{3}\frac{\hat{k}^2}{\mu-1}} \right)$$

$$= \delta_{\tilde{\boldsymbol{k}},\mathbf{0}} \cdot \mu(\mu-1) \cdot w\left(\frac{\hat{k}^2}{2(\mu-1)} \right), \tag{21}$$

with the gel fraction approximately given by $Q \approx 2(\mu-1)$. The scaling function $\omega(x)$ is defined in Ref. 12 (see Appendix C 1 for details); for convenience we define the shorthand $w(x) := \omega(\sqrt{8x/3})$.

C. Stability of the homogeneously mixed gel

Starting from a gel prepared from a homogeneous melt, i.e., $\chi_p < 1/(1-q^2)$, we now allow the incompatibility to be changed after cross-linking. In order to keep the gel homogeneous, χ_m must remain smaller than the critical value χ_{crit} for (micro-)phase separation. As can be seen from the term coupling $\Psi_{\boldsymbol{k}}$ and $\Omega_{\hat{k}}$ in the effective free energy (19), the gel network stabilizes the mixed state; the details are discussed in the following.

As long as the gel is homogeneous, the order parameter (21) solves the stationarity conditions (17). To determine the stability of the mixed state, we need the second derivative of $\mathcal{F}_n$ with respect to the charge density, evaluated at the saddle point. We restrict the discussion to a weak gel, i.e., $\mu - 1 \ll 1$, so that the saddle point value of $\Omega_{\hat{k}}$ is small and the Hessian can be approximated by its expansion to linear order in $\bar{\Omega}_{\hat{k}}$. It then can be read off from the Landau expansion (19) with $\Omega_{\hat{k}}$ replaced by the explicit saddle point value (21). The latter vanishes unless $\tilde{\boldsymbol{k}} = 0$: hence there is no coupling between the different $\boldsymbol{k}$'s, and the Hessian can be calculated independently for each wave vector. We obtain

$$\left. \frac{\partial^2 \mathcal{F}_n}{\partial \Psi_{\boldsymbol{k}}^{\alpha_1} \partial \Psi_{-\boldsymbol{k}}^{\alpha_2}} \right|_{\bar{\Psi},\bar{\Omega}} \approx N(1-q^2) \cdot A_{\alpha_1\alpha_2}(k), \tag{22}$$

where

$$A_{\alpha_1\alpha_2} := \begin{pmatrix} c & -b & \cdots & -b \\ -b & a & \ddots & \vdots \\ \vdots & \ddots & \ddots & -b \\ -b & \cdots & -b & a \end{pmatrix} \tag{23}$$

with

$$a := \left(\frac{1}{(1-q^2)\chi_m} - g_D(k^2) \right),$$

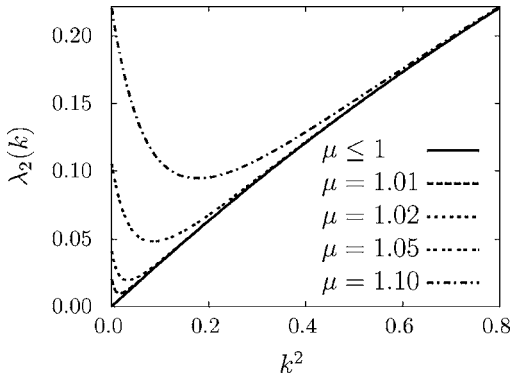

FIG. 1. Stability parameter $\lambda_2(k)$ for $\chi_m = 1/(1-q^2)$ as a function of k^2.

$$b := \mu(\mu-1) w(k^2/(\mu-1)),$$

and

$$c := \left(\frac{1}{(1-q^2)\chi_p} - g_D(k^2) \right). \tag{24}$$

The stability of the homogeneous state is equivalent to the positivity of $\mathbf{A}$. In the limit $n \to 0$, its eigenvalues are given by

$$\lambda_1(k) := c \quad \text{(nondegenerate)} \tag{25}$$

and

$$\lambda_2(k) := a + b \quad (n - \text{fold degenerate}). \tag{26}$$

As we assume cross-linking in the mixed phase, λ_1 is always positive, and thus the stability condition reduces to $\lambda_2 > 0$ or, equivalently, $\chi_m < \chi_{\mathrm{crit}}(\mu)$ with

$$(1-q^2)\chi_{\mathrm{crit}}(\mu) := 1/\max_k \{ g_D(k^2) - \mu(\mu-1) w(k^2/(\mu-1)) \}. \tag{27}$$

Figure 1 shows $\lambda_2(k)$ for $\chi_m = 1/(1-q^2)$ and different cross-link concentrations. Increasing χ_m shifts the curve downwards. Apparently, an instability towards demixing first occurs for a nonzero wave number k_c, which maximizes the above expression.

We consider the case of a weak gel, so $\mu(\mu-1) \approx \mu - 1$, and we can write $g_D(k^2) \approx 1 - k^2/3$ as the Debye function decays much more slowly than $w(k^2/(\mu-1))$. In this approximation, k_c is given by

$$0 = \left. \frac{\partial \lambda_2}{\partial k^2} \right|_{k=k_c} \approx \frac{1}{3} + w'\left(\frac{k_c^2}{(\mu-1)} \right), \tag{28}$$

which leads to $k_c^2 \approx 1.61(\mu-1)$ and $(1-q^2)\chi_{\mathrm{crit}} - 1 \approx k_c^2/3 + (\mu-1) w(k_c^2/(\mu-1) r) \approx 0.98(\mu-1)$.

A more precise numerical analysis without these approximations yields

$$(1-q^2)\chi_{\mathrm{crit}} - 1 = 0.98 \cdot (\mu-1) + 0.70 \cdot (\mu-1)^2 + \mathcal{O}((\mu-1)^3) \tag{29}$$

and

$$k_c^2 = 1.61 \cdot (\mu-1) + 1.75 \cdot (\mu-1)^2 + \mathcal{O}((\mu-1)^3). \tag{30}$$

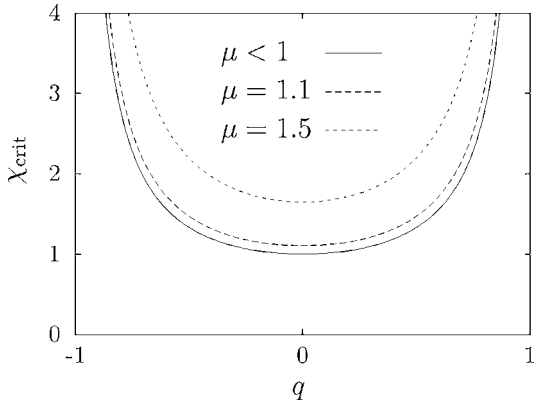

FIG. 2. Stability limits $\chi_{crit}(\mu)$ as a function of the asymmetry q for the liquid ($\mu<1$) and gels with different strengths ($\mu=1.1$ and $\mu=1.5$).

The instability for nonzero k implies that the gel undergoes microscopic (rather than macroscopic) phase separation. This is to be expected, because cross-links permanently connect different chains and thus prevent true macroscopic phase separation. The "next best"state for the system is phase separation up to the length scale of the network, i.e., the typical mesh size, as given by the average localization length $\bar{\xi}\sim(\mu-1)$. Hence the instability occurs at a critical wave number $k_c\sim 1/\bar{\xi}$.

The instability is hampered by an increased density μ of cross-links and the asymmetry q of the composition. The spinodals for the liquid blend and two solid gels with two different degrees of cross-linking are shown in Fig. 2 as a function of q. In contrast, the critical wave number remains unchanged in agreement with the above argument—the critical wave number is determined by the mesh size, which is unaffected by q. The microphase transition is addressed in Sec. V, where it will be shown that the average charge also influences the observed microstructure.

D. Pseudo phase diagram

Three parameters determine the state of the system: μ controls the number of cross-links, χ_p specifies the charge fluctuations at preparation, and χ_m the charge fluctuations after the gel has been prepared. Each of them can be chosen such that the system is close to a critical point: $\mu=1$ corresponds to the gelation transition, $\chi_p=1/(1-q^2)$ to macroscopic phase separation in the preparation ensemble, and $\chi_m=\chi_{crit}$ to microphase separation in the gel.

In Fig. 3 we show a phase diagram in the χ_m-μ plane for the special case $q=0$. [The spinodals of the asymmetric case can be recovered by replacing χ by $(1-q^2)\chi$.] The dashed line $\mu=1$ separates the gel state and the liquid state. The latter is further divided into a mixed and a macroscopically phase separated liquid at $\chi_m=1$ (solid line). The dotted line $\chi_m=\chi_{crit}$ separates the mixed gel from the microphase separated one.

The diagram in Fig. 3 is not a true equilibrium phase diagram, because the state of the system also depends on the preparation ensemble via χ_p. In particular, the microphases are only obtained if cross-linking takes place in the homogeneously mixed phase. As a consequence, the transition line

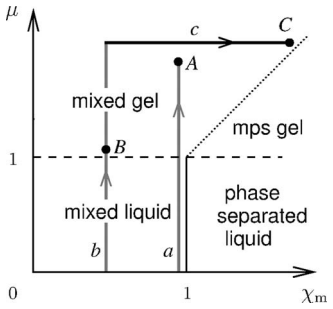

FIG. 3. Pseudo phase diagram of the polymer blend in the χ-μ plane. The state of the system is, however, history dependent (see text for details).

$\mu=1$ cannot be crossed from the macro- to the microphase separated state for $\chi_m>1$. The history of the gel is indicated by a *path* in the diagram. Of particular interest are the three paths a, b, and c. Path a amounts to cross-linking close to macroscopic phase separation, $\chi_p\to 1$, and the end point A corresponds to a homogeneously mixed gel having long-ranged frozen-in charge fluctuations. Along path b the system is cross-linked in a preparation state that is far away from macroscopic phase separation. The end point B corresponds to a homogeneously mixed and rather weak gel, just cross-linked enough to be solidlike. Along path c, the system is prepared in the same way as on path b, however, more cross-links are introduced, which strengthen the gel. Subsequently, the temperature is lowered (the incompatibility χ_m increased), so that the end point C is close to microphase separation. These three histories are representative in the following sense. Each end point corresponds to a state close to one critical point, as discussed above: point A is close to macroscopic phase separation in the preparation ensemble, $\chi_p=1$; point B is close to the gelation transition, $\mu=1$; and point C is close to microphase separation, $\chi_m=\chi_{crit}$. The three states of the system, corresponding to the end points, will be discussed in detail in the following sections.

E. Charge density correlations in the mixed gel

In this section we discuss the homogeneously mixed gel phase, for which the order parameter for phase separation vanishes. Nevertheless, there are thermal as well as quenched charge fluctuations on various length scales. These can be detected with the help of multiple correlation functions. On the Gaussian level of approximation, these correlation functions are given by the inverse of the Hessian matrix (23) as follows:

$$\langle\Psi_{-k}^{\alpha_1}\Psi_{k}^{\alpha_2}\rangle_{n+1}^{\mathcal{F}}=(A^{-1})_{\alpha_1\alpha_2}. \tag{31}$$

The correlator that is off-diagonal in replica space accounts for the frozen-in correlations and will be termed the *glassy* correlator. It is given by

$$S_{gl}(k):=[\langle\tilde{\Psi}_{-k}\rangle\langle\tilde{\Psi}_{k}\rangle]=\lim_{n\to\infty}\langle\Psi_{k}^{\alpha}\Psi_{-k}^{\beta}\rangle=\frac{1}{\chi_m^2}\cdot\frac{b(b+c)}{c\cdot\lambda_2^2}; \tag{32}$$

see Eq. (8) for the definition of $\tilde{\Psi}$. The replica-diagonal correlator is the *scattering intensity*

$$S_{\mathrm{sc}}(k) := [\langle \tilde{\Psi}_{-\boldsymbol{k}} \tilde{\Psi}_{\boldsymbol{k}} \rangle] = \lim_{n\to 0} \langle \Psi_{\boldsymbol{k}}^{\alpha} \Psi_{-\boldsymbol{k}}^{\alpha} \rangle$$
$$= \frac{1}{\chi_m^2} \left(\frac{b(b+c)}{c \cdot \lambda_2^2} + \frac{1}{\lambda_2} - \chi_m \right), \qquad (33)$$

and the *variance* (or connected correlator) is given by

$$S_{\mathrm{var}}(k) := S_{\mathrm{sc}}(k) - S_{\mathrm{gl}}(k) = \frac{1}{\chi_m^2} \cdot \left(\frac{1}{\lambda_2} - \chi_m \right). \qquad (34)$$

Whereas the *glassy correlator* $S_{\mathrm{gl}}(k)$ describes the static, frozen-in correlations, the variance $S_{\mathrm{var}}(k)$ quantifies the volatile, thermal fluctuations about the mean value. The scattering intensity $S_{\mathrm{sc}}(k)$ is the sum of both contributions and covers both thermal and static charge inhomogeneities.

1. Restriction to symmetric blends

In the following discussion of $S_{\mathrm{sc}}(k)$, $S_{\mathrm{gl}}(k)$, and $S_{\mathrm{var}}(k)$ we shall confine ourselves to the case of symmetric blends, yet without loss of generality: The scattering functions of the asymmetric case are recovered via multiplication by $\gamma=(1-q^2)$ and the rescalings $\chi_p \to \gamma\chi_p$ and $\chi_m \to \gamma\chi_m$. Furthermore, the distance to phase separation is replaced with the distance to the spinodal in the asymmetric case. In the range between the equilibrium phase transition and the spinodal, the results then describe an undercooled mixture.

2. Length scales

The correlation functions are characterized by three length scales which are determined by the parameters (μ, χ_p, χ_m) of preparation and measurement conditions.

First, there is the typical localization length ξ of the monomers in the gel fraction, i.e., the mean mesh size of the gel. From Eq. (21) we can infer that this length scale is roughly given by

$$\xi_l := 1/\sqrt{\mu - 1}. \qquad (35)$$

Second, there is the decay length ξ_p of the precritical demixing fluctuations prior to gelation. This approximately reads

$$\xi_p := 1/\sqrt{1 - \chi_p}. \qquad (36)$$

The third length characterizes the precritical fluctuations of microphase separation, and is approximately given by

$$\xi_m := 1/\sqrt{\chi_{\mathrm{crit}}(\mu) - \chi_m}. \qquad (37)$$

The three length scales measure, or are given by, the inverse distance to the phase transitions of gelation and demixing in the pre-cross-linking blend, and microphase separation in the gel; hence they grow large when approaching their respective transitions. In the following, we shall essentially discuss three limiting regimes, in which the correlation functions are determined by one of the three length scales $\xi_p \gg \xi_l, \xi_m$ (point *A*), $\xi_l \gg \xi_p, \xi_m$ (point *B*), and $\xi_m \gg \xi_l, \xi_p$ (point *C*).

3. Glassy correlations

The glassy correlation function $S_{\mathrm{gl}}(k)$ describes *time-persistent* charge inhomogeneities due to cross-linking. If the preparation ensemble is close to phase separation, then instantaneous cross-linking will freeze in these fluctuations and S_{gl} will be dominated by the pre-cross-linking fluctuations, giving rise to a high value at zero wave vector. If, on the other hand, the preparation ensemble is in a well-mixed state, then cross-linking will introduce *completely random, static* charge fluctuations, which subsequently can be enhanced by approaching the microphase separation transition in the gel. In the following, we discuss the three limiting cases (i.e., points *A*, *B*, and *C*) in detail.

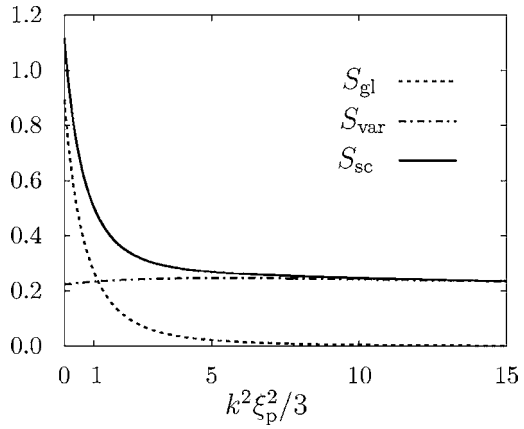

FIG. 4. Correlation functions for a *gel prepared close to phase separation*: S_{gl}, S_{var}, and S_{sc} in units of $4\xi_p^2\xi_m^4/\xi_l^4$ for $\xi_l^2=10^2$, $\xi_p^2=10^3$, and $\xi_m^2=10$.

We first consider a gel that is prepared from a melt close to phase separation, i.e., $\xi_p \gg (\xi_l, \xi_m) \gg 1$, corresponding to point *A* in Fig. 3. The network can freeze in correlations on length scales larger than or comparable to its mesh size. For $\xi_p \gg \xi_l$, the pre-cross-linking fluctuations have long enough scales to be frozen. Consequently, the glassy correlations reflect the pre-cross-linking fluctuations:

$$S_{\mathrm{gl}}(k) \propto \frac{\xi_p^2}{1 + k^2\xi_p^2/3}. \qquad (38)$$

The glassy correlations are proportional to ξ_p^2 and decay on the scale $k \sim \xi_p^{-1}$ set by the fluctuations of the preparation ensemble. An example is included in Fig. 4.

In a weak gel, i.e., if $\xi_l \gg (\xi_p, \xi_m) \gg 1$ (point *B*), the network is rather wide-meshed, so that the fluctuations at preparation cannot be frozen in. Instead, there will be static charge fluctuations $\langle \tilde{\Psi}_{\boldsymbol{k}} \rangle \neq 0$ on the scale of the network, which are completely random and hence vanish, if averaged over cross-link configurations, $[\langle \tilde{\Psi}_{\boldsymbol{k}} \rangle]=0$. They do, however, contribute to the glassy correlations, which are given approximately by

$$S_{\mathrm{gl}}(k) \approx \tfrac{1}{2} Q \xi_m^4 \cdot w(k^2\xi_l^2). \qquad (39)$$

These fluctuations always decay on the length scale of localization, but they are enhanced in magnitude when approaching microphase separation. An example of the glassy correlations in this range is given in Fig. 5.

The crossover between the two scales is demonstrated in Fig. 6, which shows $S_{\mathrm{gl}}(k)/S_{\mathrm{gl}}(0)$ far from microphase separation for $\xi_l=10$. For the leftmost curve $\xi_p^2=10^5 \gg \xi_l^2=100$, and hence the decay occurs at $k \sim \xi_p^{-1}$. Upon decreasing ξ_p,

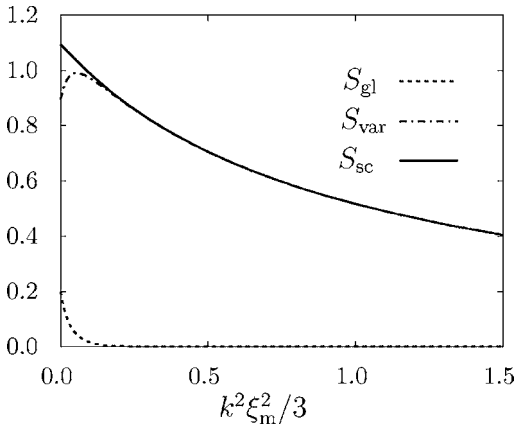

FIG. 5. Correlation functions for a *weak gel*: S_{gl}, S_{var}, and S_{sc} in units of ξ_m^2 for $\xi_l^2=10^2$, $\xi_p^2=10$, and $\xi_m^2=10$.

the curves shift to the right, until, for $\xi_l \gg \xi_p$, the decay is determined by ξ_l. The inset shows the half-width at half-maximum as a function of ξ_p^{-1}.

Close to microphase separation, i.e., $\xi_m \gg (\xi_l, \xi_p) \gg 1$ (point *C*), $S_{gl}(k)$ is dominated by the critical fluctuations towards microphase separation. In the absence of cross-links there would be large-scale fluctuations towards macroscopic demixing. In the gel, displacements are bounded by the localization length, so that $S_{gl}(k)$ develops a peak at $k_c \sim \xi_l^{-1}$, where $\lambda_2(k)$ becomes small; an example is included in Fig. 7. Approaching the transition, the peak diverges as $\lambda_2^{-2}(k)$, and the glassy correlations can be approximated by

$$S_{gl}(k) \propto \frac{Q}{\left(\chi_{crit}(\mu) - \chi_m + \frac{1}{2}(k^2-k_c^2)^2 w''(1)/k_c^2\right)^2}, \tag{40}$$

where w'' denotes the second derivative of the scaling function introduced below Eq. (21) and defined in Appendix C.

4. Thermal fluctuations

The variance $S_{var}(k)$ of the charge fluctuations is *independent* of the conditions at the time of cross-linking. Hence,

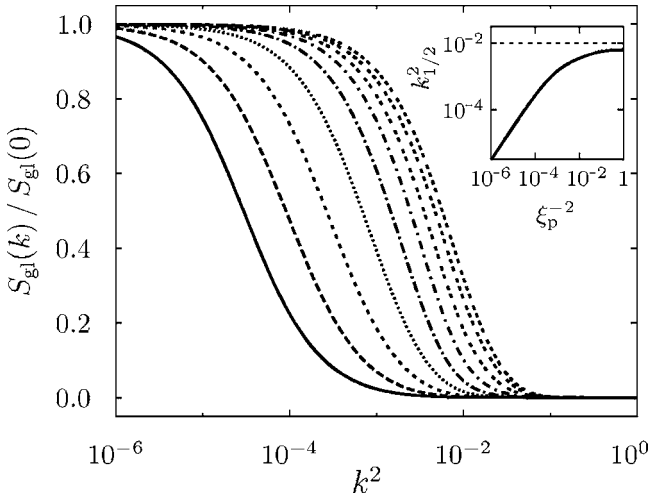

FIG. 6. Scale crossover in the glassy correlation function S_{gl}, normalized to the value at $k=0$: Crossover from preparation close to demixing to a weak gel, with $\chi_m=0.1$, $\xi_l^2=10^2$, and $\xi_p^2=10^5, 10^{4.5}, \ldots, 10^1$ (from left to right). Inset: Half-width $k_{1/2}^2$ of $S_{gl}(k)$ crossing over from ξ_p^{-2} to ξ_l^{-2} (dashed line).

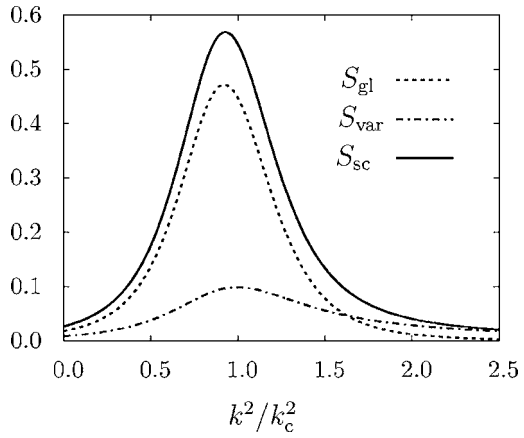

FIG. 7. Correlation functions for a *gel measured close to microphase separation*: S_{gl}, S_{var}, and S_{sc} in units of ξ_m^4/ξ_l^2 for $\xi_l^2=10^2$, $\xi_p^2=10$, and $\xi_m^2=10^3$. The wave-number squares are measured in units of k_c^2.

there are only two competing length scales, ξ_l and ξ_m. In case of a weak gel, i.e., $\xi_l \gg \xi_m \gg 1$ (point *B* in Fig. 3), Eq. (34) reduces to

$$S_{var}(k) \approx \frac{\xi_m^2}{1+k^2\xi_m^2/3} \tag{41}$$

for small k, decaying with a half-width of $k_{1/2} \approx \sqrt{3}/\xi_m^2$, provided ξ_m is not too small. Far away from the demixing threshold, the fluctuations are hardly affected by the network and look like critical fluctuations approaching macroscopic phase separation. An example is shown in Fig. 5.

Close to microphase separation, i.e., $\xi_m \gg \xi_l \gg 1$ (point *C*), the fluctuations grow with increasing k until k reaches the inverse localization length $k \sim \xi_l^{-1}$, beyond which they are strongly suppressed by the network. The variance is approximately given by

$$S_{var}(k) \approx \frac{1}{\lambda_2} \approx \frac{1}{\chi_{crit}(\mu) - \chi_m + \frac{1}{2}(k^2-k_c^2)^2 w''(1)/k_c^2}, \tag{42}$$

revealing a peak at $k_0 \sim 1/\xi_l$ that has a height proportional to ξ_m^2. See Fig. 7 for an example.

5. Scattering intensity

The behavior of the scattering function in the various regimes can be inferred from the behaviors of $S_{gl}(k)$ and $S_{var}(k)$, as $S_{sc}(k)$ is just the sum of them. A weak gel (point *B*) preserves only a small amount of the precross-linking fluctuations and can hardly restrict thermal fluctuations. Hence, $S_{sc}(k) \approx S_{var}(k)$, so the scattering function decays on the scale $k \sim \xi_m$; see Fig. 5. In the other regimes, thermal fluctuations are suppressed by the network, and $S_{sc}(k) \approx S_{gl}(k)$. In a gel *prepared* close to phase separation (point *A*), the scattering function decays on the scale $k \sim \xi_p$ (Fig. 4), whereas a gel *measured* close to microphase separation (path *C*) reveals a peak at $k \sim k_0$, diverging at the transition (Fig. 7).

V. MICROSTRUCTURES

At $\chi_m=\chi_{\rm crit}$, the homogeneous gel becomes unstable with respect to phase separation. As we have seen in Sec. IV C, the instability first occurs for nonzero wave numbers, indicating that the gel undergoes microscopic rather than macroscopic phase separation. In this section we investigate various microstructures, such as hexagons and lamellas with a definite orientation, as well as a superposition of many random orientations. The selection of a particular microstructure depends sensitively on the compressibility and the charge imbalance. We first discuss the simplest case of incompressible, symmetric mixtures, and then go on to investigate the effects of charge imbalance and compressibility.

A. Incompressible, symmetric mixtures

Our analysis of microphase separation is based on the effective free energy (14) in the gel phase. We expand it around $\Psi=0$ up to fourth order, in the presence of a nonzero gel order parameter $\bar{\Omega}$ given by Eq. (21). The expansion reads

$$\frac{n}{N}\mathcal{F}_n(\{\Psi\}) \approx \tfrac{1}{2}\sum_{\alpha_{1,2}}\sum_{\boldsymbol{k}}{}' A_{\alpha_1,\alpha_2}(k)\Psi_{\boldsymbol{k}}^{\alpha_1}\Psi_{-\boldsymbol{k}}^{\alpha_2} + \tfrac{1}{8}\sum_{\alpha}\sum_{\boldsymbol{k}_{1,2,3,4}}{}' \delta_{\boldsymbol{k}_1+\boldsymbol{k}_2+\boldsymbol{k}_3+\boldsymbol{k}_4,0}\left(\frac{g_3(\boldsymbol{k}_1,\boldsymbol{k}_2)g_3(\boldsymbol{k}_3,\boldsymbol{k}_4)}{g_D((\boldsymbol{k}_1+\boldsymbol{k}_2)^2)} - \frac{g_{\Psi^4}(\boldsymbol{k}_1,\boldsymbol{k}_2,\boldsymbol{k}_3)}{3}\right)\Psi_{\boldsymbol{k}_1}^{\alpha}\Psi_{\boldsymbol{k}_2}^{\alpha}\Psi_{\boldsymbol{k}_3}^{\alpha}\Psi_{\boldsymbol{k}_4}^{\alpha}. \tag{43}$$

Here, $A_{\alpha_1\alpha_2}(k)$ is given in Eqs. (23) and (24), and the vertex of the fourth-order term is given by the Wiener correlators

$$g_3(\boldsymbol{k}_1,\boldsymbol{k}_2) = \int_0^1 ds_1 ds_2 ds_3 \langle e^{-i\Sigma_{\nu=1}^3 \boldsymbol{k}_\nu \mathbf{r}(s_\nu)}\rangle^W \Big|_{\boldsymbol{k}_3=-\boldsymbol{k}_1-\boldsymbol{k}_2} \tag{44}$$

and

$$g_{\Psi^4}(\boldsymbol{k}_1,\boldsymbol{k}_2,\boldsymbol{k}_3) = \int_0^1 ds_1 ds_2 ds_3 ds_4 \langle e^{-i\Sigma_{\nu=1}^4 \boldsymbol{k}_\nu \mathbf{r}(s_\nu)}\rangle^W \Big|_{\boldsymbol{k}_4=-\Sigma_{\nu=1}^3 \boldsymbol{k}_\nu}. \tag{45}$$

The fourth-order term in Eq. (43) apparently depends on the spatial structure of the microphases, and is responsible for the pattern selection as well as for the wave-number selection in the microphase separated state. A particularly simple pattern are lamellas with sinusoidal modulations in real space:

$$\bar{\Psi}_{\boldsymbol{p}}^{\alpha} = \begin{cases} 0 \text{ for } \alpha = 0 \\ \sqrt{2}(\delta_{\boldsymbol{p},\boldsymbol{k}} + \delta_{\boldsymbol{p},-\boldsymbol{k}})\psi \quad \text{otherwise}. \end{cases} \tag{46}$$

This ansatz is replica symmetric, apart from the zeroth replica, which reflects the preparation ensemble. The wavelength $2\pi/k$ and the amplitude $\psi \geqslant 0$ are variational parameters subject to optimization. Insertion into (43) yields

$$f(\{\Psi\}) := \frac{1}{N}\cdot\lim_{n\to 0}\mathcal{F}_n(\{\Psi\}) \approx \lambda_2(k^2)\cdot\psi^2 + \frac{1}{2}g_4(k^2)\cdot\psi^4, \tag{47}$$

with λ_2 defined in Eq. (26) and

$$g_4(k^2) := \frac{1}{2}\left(\frac{(g_3(\boldsymbol{k},\boldsymbol{k}))^2}{g_D(4k^2)} + 2(g_D(k^2))^2 - g_{\Psi^4}(\boldsymbol{k},\boldsymbol{k},-\boldsymbol{k})\right) = 1 - \frac{2}{3}k^2 + \mathcal{O}(k^4) \tag{48}$$

(see Appendix B).

At the onset of the microphases, the amplitude goes to zero continuously, and the optimal wave number is given by k_c [see Eq. (30)], implying a domain size of the order of the localization length of the gel. Beyond the critical point, the amplitude is nonzero, and the wave number deviates from its critical value k_c. Both are obtained from a variational optimization of the above free energy:

$$\psi_{\rm min}^2(k) = -\frac{\lambda_2(k)}{g_4(k^2)} \quad \text{and} \quad k_{\rm min}^2 - k_c^2 = c_0\cdot(\chi_m-\chi_{\rm crit}) + \mathcal{O}((\chi_m-\chi_{\rm crit})^2). \tag{49}$$

The constant c_0 can be computed analytically only for a weak gel, by further expansion in powers of $\mu-1$, which yields $c_0 \approx 1.09(\mu-1)$. The optimal amplitude $\psi_{\rm min}(k_{\rm min})$ grows continuously with $\chi_m-\chi_{\rm crit}$ as follows:

$$\psi_{\rm min}^2 = \frac{\chi_m-\chi_{\rm crit}}{\chi_{\rm crit}^2\, g_4(k_c^2)} + \mathcal{O}((\chi_m-\chi_{\rm crit})^2). \tag{50}$$

Other simple structures, such as a hexagonal stack of cylinders or a bcc crystal of spheres, have higher free energies. The same holds for a superposition of several sinusoidal modulations like Eq. (46), with the same wave numbers but different directions. As we shall see below, these conclusions depend on the symmetry of the mixture and its compressibility.

B. Effects of asymmetry

The most important effect of the asymmetry is a third-order term in the Landau expansion, rendering both the mac-

rophase separation of the uncross-linked liquid and the microphase separation of the gel first-order transitions.

To keep the discussion simple, we neglect deviations of k^2 from k_c^2 and drop the k dependence of the higher-order terms in the Landau free energy. With the ansatz $\Psi_{\boldsymbol{k}}^{\alpha}=(1-\delta_{\alpha,0})\Psi_{\boldsymbol{k}}$, corresponding to the mixed state in the preparation ensemble and replica-symmetric phase separation in the measurement ensemble, this leads to the free energy density

$$\begin{aligned}\frac{f(\{\Psi\})}{1-q^2} &= \tfrac{1}{2}{\sum_{\boldsymbol{k}}}' \lambda_2(k)\Psi_{\boldsymbol{k}}\Psi_{-\boldsymbol{k}} \\ &+ \frac{q}{3}{\sum_{\boldsymbol{k}_{1,2,3}}}' \Psi_{\boldsymbol{k}_1}\Psi_{\boldsymbol{k}_2}\Psi_{\boldsymbol{k}_3}\cdot\delta_{\boldsymbol{k}_1+\boldsymbol{k}_2+\boldsymbol{k}_3,\boldsymbol{0}} \\ &+ \frac{q^2}{2}\left({\sum_{\boldsymbol{k}}}' \Psi_{\boldsymbol{k}}\Psi_{-\boldsymbol{k}}\right)^2 \\ &+ \frac{1-3q^2}{12}{\sum_{\boldsymbol{k}_{1,2,3,4}}}' \Psi_{\boldsymbol{k}_1}\Psi_{\boldsymbol{k}_2}\Psi_{\boldsymbol{k}_3}\Psi_{\boldsymbol{k}_4}\cdot\delta_{\boldsymbol{k}_1+\boldsymbol{k}_2+\boldsymbol{k}_3+\boldsymbol{k}_4,\boldsymbol{0}},\end{aligned} \tag{51}$$

with $\lambda_2(k)$ defined in Eq. (26).

Besides the lamellar microphases already discussed in Sec. V, we now consider two additional morphologies: Cylindrical phases having parallel orientation, aligned on a honeycomb lattice in the perpendicular plane, and spherical domains on a body centered cubic lattice. Although a randomly cross-linked blend will probably reveal only local order, the regular structures are useful for constructing a simple and tractable ansatz for the microphase separated state:

$$\Psi_{\boldsymbol{p}} = \frac{\Psi}{\sqrt{m}}\sum_{i=1}^{m}(\delta_{\boldsymbol{p},k\mathbf{n}_i}+\delta_{\boldsymbol{p},-k\mathbf{n}_i}) \tag{52}$$

with $m=1$ for lamellas, $m=3$ for hexagonally ordered cylinders, and $m=6$ for spheres on a bcc lattice, and the corresponding lattice vectors $\{\boldsymbol{n}_i\}$ being defined in Appendix A 1.

With the lattice ansatz (52), the evaluation of the higher-order sums in Eq. (51) amounts to counting the number of possible "loops"of two, three, and four lattice vectors that add to zero. This is carried out in Appendix A 1 a, yielding ${\Sigma_{\boldsymbol{k}}}' \Psi_{\boldsymbol{k}}\Psi_{-\boldsymbol{k}}=2\Psi^2$, independent of the morphology, and also

$${\sum_{\boldsymbol{k}_{1,2,3}}}' \Psi_{\boldsymbol{k}_1}\Psi_{\boldsymbol{k}_2}\Psi_{\boldsymbol{k}_3}\cdot\delta_{\boldsymbol{k}_1+\boldsymbol{k}_2+\boldsymbol{k}_3,\boldsymbol{0}} = c_3^{(m)}\Psi^3, \tag{53}$$

$${\sum_{\boldsymbol{k}_{1,2,3,4}}}' \Psi_{\boldsymbol{k}_1}\Psi_{\boldsymbol{k}_2}\Psi_{\boldsymbol{k}_3}\Psi_{\boldsymbol{k}_4}\cdot\delta_{\boldsymbol{k}_1+\boldsymbol{k}_2+\boldsymbol{k}_3+\boldsymbol{k}_4,\boldsymbol{0}} = c_4^{(m)}\Psi^4, \tag{54}$$

where

$$c_3^{(1)}=0, \quad c_3^{(3)}=4/\sqrt{3}, \quad c_3^{(6)}=4\sqrt{2/3}, \tag{55}$$

$$c_4^{(1)}=6, \quad c_4^{(3)}=10, \quad c_4^{(6)}=15. \tag{56}$$

Thus, the free-energy density becomes

$$\begin{aligned}\frac{f(\{\Psi\})}{1-q^2} &= \frac{\chi_m^{-1}-\chi_{\mathrm{crit}}^{-1}}{1-q^2}\cdot\Psi^2+\frac{qc_3^{(m)}}{3}\cdot\Psi^3 \\ &+\left(2q^2+\frac{(1-3q^2)c_4^{(m)}}{12}\right)\cdot\Psi^4.\end{aligned} \tag{57}$$

Here, λ_2 has been evaluated at k_c because (in this section) we are not considering deviations of the wave number from its critical value.

For $m=1$, the third-order term vanishes, even if $q\neq 0$, so the transition remains second order and the spinodal indeed indicates the equilibrium phase transition point with respect to lamellas. In contrast, for cylinders and bcc spheres the equilibrium transition point χ_t is shifted according to

$$\begin{aligned}\frac{1}{(1-q^2)\chi_t}-\frac{1}{(1-q^2)\chi_{\mathrm{crit}}} &= \frac{(qc_3^{(m)}/3)^2}{4(2q^2+(1-3q^2)c_4^{(m)}/12)} = \frac{(qc_3^{(m)})^2}{72q^2+3(1-3q^2)c_4^{(m)}} \\ &= \begin{cases}\dfrac{8q^2}{45-27q^2}=\dfrac{24}{135}q^2+\mathcal{O}(q^4) & \text{for } m=3 \text{ (cylinders)} \\ \dfrac{32q^2}{135-189q^2}=\dfrac{32}{135}q^2+\mathcal{O}(q^4) & \text{for } m=6 \text{ (bcc spheres)}.\end{cases}\end{aligned} \tag{58}$$

In the asymmetric case, the bcc spheres yield the lowest equilibrium transition point of the three possibilities considered, i.e., microphases first occur with bcc symmetry. This is to be expected, as the ratio of surface to volume of the minority phases is minimal for spheres embedded in the majority phase, and is in agreement with the finding of Alexander and McTague[13] of a general preference for bcc symmetry in crystal nucleation. Note, however, that the Landau expansion is only valid for small q^2, for which the transition is weakly first order. In particular, for $q^2=5/7$, where the right hand side in the last line of Eq. (58) diverges, the Landau expansion breaks down.

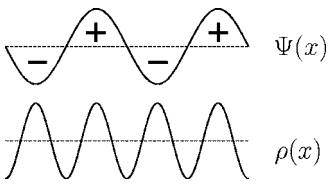

FIG. 8. Coupling of mass (ρ) and charge (Ψ) densities. Zones of large charge-density modulation are condensed, hence the mass density is modulated with half the wavelength of the charge-density modulations.

C. Effects of compressibility

A compressible system can avoid unfavorable A-B contacts and lower its energy by diluting mixed regions having many such contacts, which are characterized by a small absolute charge density, and condensing regions that are rich in either A or B, which have a high absolute charge density. Mathematically, this becomes apparent via a nonzero value of the saddle point of the density $\bar{\rho}$ in a phase separated state. For simplicity, we restrict the discussion of compressibility effects to the symmetric case, where the shifted and the original density fields coincide. In this case, the saddle point of ρ is given by

$$\bar{\rho}_{\boldsymbol{k}}^{\alpha} = \frac{i}{2(1/\tilde{\lambda}^{\alpha} + g_D(k^2))} \sum_{k_{1,2}}{}' \Psi_{\boldsymbol{k}_1}^{\alpha} \Psi_{\boldsymbol{k}_2}^{\alpha} \cdot \delta_{\boldsymbol{k}+\boldsymbol{k}_1+\boldsymbol{k}_2,\boldsymbol{0}}. \tag{59}$$

For the simple example of lamellar microphases described by a single wave vector $\boldsymbol{k}$ as in Eq. (46), Eq. (59) predicts density-field modulations having wave vector $\boldsymbol{k}_1 = \pm 2\boldsymbol{k}$, i.e., with twice the wave number of the charge-density modulations. This is intuitively clear: Along one spatial period of the charge-density modulations, their modulus or square, and thus the mass density, oscillates twice, corresponding to the half-wavelength or the double wave number; this is illustrated in Fig. 8.

The compressibility is controlled by the strength of the excluded volume interaction, i.e., the parameter $\tilde{\lambda} = \lambda_m - \mu/V^m$. To study microphase separation in the symmetric but compressible case, we integrate out the density field, keeping $\tilde{\lambda}$ finite. With the ansatz $\Psi^{\alpha} = (1 - \delta_{\alpha,0})\Psi$, we obtain

$$f(\Psi) = \frac{1}{2}\sum_{\boldsymbol{k}}{}' \lambda_2(k) \Psi_{\boldsymbol{k}} \Psi_{-\boldsymbol{k}} + \frac{1}{8\lambda_{\text{eff}}} \left(\sum_{\boldsymbol{k}}{}' \Psi_{\boldsymbol{k}} \Psi_{-\boldsymbol{k}} \right)^2 + \frac{1}{12} \left(1 - \frac{3}{2\lambda_{\text{eff}}} \right) \sum_{k_{1,2,3,4}}{}' \Psi_{\boldsymbol{k}_1} \Psi_{\boldsymbol{k}_2} \Psi_{\boldsymbol{k}_3} \Psi_{\boldsymbol{k}_4} \delta_{\boldsymbol{k}_1+\boldsymbol{k}_2+\boldsymbol{k}_3+\boldsymbol{k}_4,\boldsymbol{0}}. \tag{60}$$

Here, $\lambda_{\text{eff}} = \lambda - \mu + 1$, and we have dropped the k dependence in the higher-order vertices, thereby restricting the domain size to its critical value, determined by k_c or the localization length of the gel.

To account for the potential randomness of the microphase pattern, we extend the previous lamellar ansatz by allowing a superposition of Z one-dimensional waves, each with identical wave number k_c but random phases Φ_z and wave-vector orientations $\boldsymbol{n}_z$, i.e.,

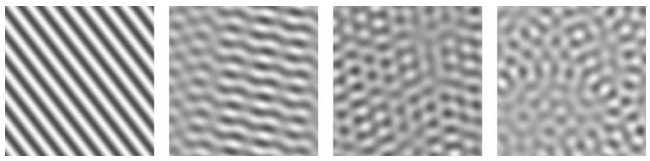

FIG. 9. Superposition of lamellæ having random orientations in real space in two dimensions. The pictures show an area of 10×10 wavelengths, and the local amplitude is indicated by the grey scale in arbitrary units for $Z = 1$, 5, 10, and 100 orientations.

$$\Psi_{\boldsymbol{k}} = \frac{\Psi}{\sqrt{Z}} \sum_{z=1}^{Z} (e^{i\Phi_z} \delta_{\boldsymbol{k},-k_c\boldsymbol{n}_z} + e^{i\Phi_z} \delta_{\boldsymbol{k},k_c\boldsymbol{n}_z}), \tag{61}$$

corresponding to $2\Psi/(VZ^{1/2}) \cdot \Sigma_{z=1}^{Z} \cos(k_c \boldsymbol{n}_z \boldsymbol{x} + \Phi_z)$ in real space. The optimal number of orientations will be determined later. A few examples of such random morphologies are shown in Fig. 9, the number of phases ranging from 1 to 100.

We assume that none of the orientations $\boldsymbol{n}_z$ are collinear, and thus the quadratic sums in Eq. (60) yield

$$\sum_{\boldsymbol{k}}{}' \lambda_2(k_c) \Psi_{\boldsymbol{k}} \Psi_{-\boldsymbol{k}} = 2\lambda_2(k_c)\Psi^2 \quad \text{and} \quad \sum_{\boldsymbol{k}}{}' \Psi_{\boldsymbol{k}} \Psi_{-\boldsymbol{k}} = 2\Psi^2. \tag{62}$$

To compute the fourth-order sum in Eq. (60), we have to count the number of possible closed loops of orientations. Because of the randomness, the existence of quadruples of orientations able to form a closed loop is very unlikely, except for the degenerate planar case of pairs of opposite vectors $(\pm\boldsymbol{n}_z, \pm\boldsymbol{n}_{z'})$, and hence we disregard nonplanar loops. Single orientations allow for the construction of quadruples $(\boldsymbol{n}_z, \boldsymbol{n}_z, -\boldsymbol{n}_z, -\boldsymbol{n}_z)$ that can be ordered in $\binom{4}{2} = 6$ ways. Quadruples $(\pm\boldsymbol{n}_z, \pm\boldsymbol{n}_{z'})$ of two pairs of different orientations can be ordered in $4! = 24$ different ways, and there are $\frac{1}{2}Z(Z-1)$ such pairs. Thus, the quartic sum in Eq. (60) yields

$$\sum_{k_{1,2,3,4}}{}' \Psi_{\boldsymbol{k}_1} \Psi_{\boldsymbol{k}_2} \Psi_{\boldsymbol{k}_3} \Psi_{\boldsymbol{k}_4} \cdot \delta_{\boldsymbol{k}_1+\boldsymbol{k}_2+\boldsymbol{k}_3+\boldsymbol{k}_4,\boldsymbol{0}} = \frac{12Z(Z-1) + 6Z}{Z^2} \Psi^4 = 12\left(1 - \frac{1}{2Z}\right)\Psi^4. \tag{63}$$

Inserting the sums into the free-energy density we obtain

$$f(\Psi) = \lambda_2(k)\Psi^2 + \left(\left(1 - \frac{1}{\lambda_{\text{eff}}}\right) - \left(1 - \frac{3}{2\lambda_{\text{eff}}}\right) \frac{1}{2Z} \right) \Psi^4. \tag{64}$$

The fourth-order term depends on λ_{eff} and the number of components Z. It has to be positive to guarantee stability, and this requires $\lambda_{\text{eff}} > 1$. The sign of the $\mathcal{O}(Z^{-1})$ term determines the optimal number of random orientations. For low compressibilities, i.e., for $\lambda_{\text{eff}} > 3/2$, the term is negative and the free energy grows with an increasing number of orientations, hence the simple lamellar morphology is favored. For a rather compressible system having, in contrast, $1 < \lambda_{\text{eff}} < 3/2$, the effective free energy decreases with increasing Z, favoring an "infinite" number of orientations and hence a random pattern.

D. Fluctuations about the microphase separated state

In this section we address the Gaussian fluctuations about the microphase separated state. Concentrating on the case of an incompressible symmetric gel, we decompose the replicated charge density field

$$\Psi_{\boldsymbol{p}}^{\alpha} = \bar{\Psi}_{\boldsymbol{p}}^{\alpha} + \Phi_{\boldsymbol{p}}^{\alpha}, \tag{65}$$

i.e., into the saddle point value $\bar{\Psi}_{\boldsymbol{p}}^{\alpha}$ (lamellas) given by Eq. (46) and the fluctuations $\Phi_{\boldsymbol{p}}^{\alpha}$ about this state. Like in the homogeneous case, the thermal fluctuations and persistent correlations of the physical charge density are given by the replica-diagonal and off-diagonal correlations $\langle \Phi_{\boldsymbol{p}}^{\alpha} \Phi_{-\boldsymbol{p}}^{\alpha} \rangle$ and $\langle \Phi_{\boldsymbol{p}}^{\alpha} \Phi_{-\boldsymbol{p}}^{\beta} \rangle$, respectively (see Sec. IV E). To compute these quantities on the Gaussian level, we require the second-order expansion of the effective free energy in terms of Φ. Insertion of Eq. (65) into Eq. (43) yields

$$\frac{n}{N}\mathcal{F}_n(\{\Phi\}) \approx \tfrac{1}{2}\sum_{\alpha_{1,2}} {\sum_{\boldsymbol{p}}}' A_{\alpha_1\alpha_2}(p)\Phi_{\boldsymbol{p}}^{\alpha_1}\Phi_{-\boldsymbol{p}}^{\alpha_2} + \psi^2 \cdot \sum_{\alpha>0} {\sum_{\boldsymbol{p}_{1,2}}}' B(\boldsymbol{k},\boldsymbol{p}_1,\boldsymbol{p}_2)\Phi_{\boldsymbol{p}_1}^{\alpha}\Phi_{\boldsymbol{p}_2}^{\alpha}, \tag{66}$$

where A_{α_1,α_2} denotes the matrix defined in Eq. (23) describing the stability of and the fluctuations in the homogeneous gel ($\chi_m < \chi_{\rm crit}$); ψ and $\boldsymbol{k}$ denote the saddle point amplitude and wave vector of the lamellar microphases, respectively. The coefficient $B(\boldsymbol{k},\boldsymbol{p}_1,\boldsymbol{p}_2)$ of the second term originates from the coupling of the fluctuations to the underlying lamellar pattern; the details of the free-energy expansion are given in Appendix D.

Besides a part diagonal in momentum space ($\boldsymbol{p}_1+\boldsymbol{p}_2=0$), the second term of Eq. (66) also includes off-diagonal terms with $\boldsymbol{p}_1+\boldsymbol{p}_2=\pm 2\boldsymbol{k}$, which can be treated perturbatively. Due to momentum conservation in the desired correlators, the off-diagonal terms do not contribute to lowest order in perturbation theory. In the vicinity of the microphase transition we find in leading order

$$\frac{n}{N}\mathcal{F}_n(\{\Phi\}) \approx \tfrac{1}{2}\sum_{\alpha_{1,2}} {\sum_{\boldsymbol{p}}}' \tilde{A}_{\alpha_1\alpha_2}(p)\Phi_{\boldsymbol{p}}^{\alpha_1}\Phi_{-\boldsymbol{p}}^{\alpha_2} + \mathcal{O}(\psi^4) \tag{67}$$

with

$$\tilde{A}_{\alpha_1\alpha_2}(\boldsymbol{p}) = A_{\alpha_1\alpha_2}(p) + \delta_{\alpha_1,\alpha_2}(1-\delta_{\alpha_1,0})\cdot 2\Psi^2 \times\left(g_D(k^2)g_D(p^2)\,\mathrm{f}+ \frac{2(g_3(\boldsymbol{k},\boldsymbol{p}))^2}{g_D((\boldsymbol{k}+\boldsymbol{p})^2)} - g_{\Psi^4}(\boldsymbol{k},-\boldsymbol{k},\boldsymbol{p})\right); \tag{68}$$

here we have used the detailed form of $B(\boldsymbol{k},\boldsymbol{p}_1,\boldsymbol{p}_2)$ given in Appendix D. In weakly cross-linked gels the dominant wave numbers $p \approx k_c$ are small, so the term in the large brackets in Eq. (68) can be expanded about $\boldsymbol{k},\boldsymbol{p}=0$, which leads to

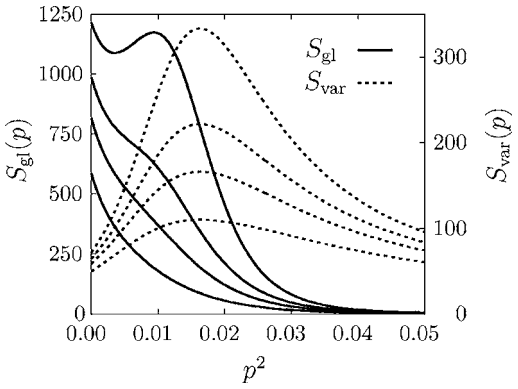

FIG. 10. Fluctuations about the microphase separated state: $S_{\rm gl}(p)$ and $S_{\rm var}(p)$ (different scales) for $\mu=1.01$, $\chi_p=0.998$, and $\chi_m/\chi_{\rm crit}=1.001$, 1.0015, 1.002, and 1.003 (from top to bottom).

$$g_D(k^2)g_D(p^2) + \frac{2(g_3(\boldsymbol{k},\boldsymbol{p}))^2}{g_D((\boldsymbol{k}+\boldsymbol{p})^2)} - g_{\Psi^4}(\boldsymbol{k},-\boldsymbol{k},\boldsymbol{p}) \approx 2 - \frac{2}{3}(k^2+p^2) + \ldots\,. \tag{69}$$

In this approximation, the angle between $\boldsymbol{p}$ and $\boldsymbol{k}$ no longer appears and the Gaussian persistent and thermal fluctuations are given by Eqs. (32)–(34), with λ_2 replaced by the corresponding eigenvalue of the matrix $\tilde{\mathbf{A}}$:

$$\tilde{\lambda}_2(p) \approx \lambda_2(p) + 4\psi^2\left(1-\frac{1}{3}(k^2+p^2)\right) \approx \lambda_2(p) - \frac{4\lambda_2(k_c)}{g_4(k_c^2)}\left(1-\frac{1}{3}(k_c^2+p^2)\right). \tag{70}$$

In the last step, we have inserted the saddle point values for the wave number and amplitude of the lamellas, $k \approx k_c$ and $\psi=\psi_{\rm min}$.

Both numerical analysis and estimations show that $\tilde{\lambda}_2$ is positive, i.e., the lamellar state is stable against fluctuations. Hence the Gaussian fluctuations do not destroy the lamellar microstructure.

Figure 10 shows an example of the persistent and thermal correlation functions of a gel prepared relatively close to demixing, measured at different distances to the microphase transition. Close to the transition, the correlation functions are strongly peaked near $p=k_c$. On raising $(\chi_m-\chi_{\rm crit})$, both correlation functions become smaller. Whereas the thermal fluctuations remain peaked at $p \approx k_c$, the persistent correlations are increasingly dominated by the frozen-in fluctuations that decay with p.

VI. CONCLUSIONS

In this paper we have analyzed a microscopic model of cross-linked polymer blends, built on the Edwards model for a polymer melt and generalized to two components, which are mutually incompatible. Random cross-links are introduced according to the Deam-Edwards distribution, also generalized to include concentration fluctuations at the instant of cross-linking. Thereby, the concentration fluctuations in the melt are partially frozen in and sustained in the gel phase.

Apart from these correlations, which are present at preparation, the cross-links are taken to connect monomers irrespective of their charge. Hence, within the mean-field theory, the resulting gel is identical to the one made from just one species of polymer. However, concentration fluctuations are present and have been computed on the Gaussian level of approximation. Of particular interest are the frozen-in or glassy fluctuations, which reflect the preparation state. In general, the network can only quench fluctuations on length scales larger than its own mesh size, which is roughly given by the localization length of the mean-field theory. If the preparation ensemble is close to macroscopic phase separation, then the length scale of these fluctuations is large compared to the mesh size, so that the glassy fluctuations are given by the concentration fluctuations in the preparation state. If, on the other hand, the preparation state is far from phase separation, the frozen-in charge fluctuations follow the network pattern, and hence are completely random, because the cross-links are not sensitive to the species. The thermal concentration fluctuations are independent of the preparation state.

Lowering the temperature in the gel, or equivalently increasing the incompatibility of the two species, gives rise to phase separation, the spatial extent of which is limited by the mesh size of the network. The length scale of the resulting "microphases" can thus range from almost microscopic to nearly macroscopic scales, depending on the degree of cross-linking of the gel. The instability towards microphase separation is signaled by a divergence of the time-persistent as well as thermal fluctuations. The emergent microstructure is shown to depend sensitively on charge imbalance and compressibility. The latter allows for random patterns with a unique wavelength, i.e., the localization length, whereas in the incompressible system lamellas are favorable for balanced mixtures and hexagonal patterns for imbalancd mixtures.

We now compare our results to previous phenomenological approaches, many of which have focused on the issue of microphase separation. de Gennes argued that the charges in the cross-linked gel cannot move freely, but are displaced in analogy to the charges in a dielectric material. He introduced a polarization $\boldsymbol{P}$ which, as in electrostatics, is determined by the charges according to $\nabla\cdot\boldsymbol{P}=-\Psi$. In the limit of weak segregation, the free energy is quadratic in the polarization, and is simply added to the free energy of charge fluctuations, resulting in

$$f(\{\Psi\}) = \tfrac{1}{2}{\sum_{\boldsymbol{k}}}'\left(\chi_{\mathrm{crit}} - \chi_m + k^2 + \frac{C}{k^2}\right)\Psi_{\boldsymbol{k}}\Psi_{-\boldsymbol{k}}, \tag{71}$$

where C is a coefficient of "internal rigidity." The above free energy leads to an instability at finite wave number (microphase separation), but predicts that $\lim_{k\to 0} S_{\mathrm{sc}}(k)=0$, in disagreement with experiment. The nonzero scattering intensity at zero wave number is due to the frozen-in charge fluctuations present at preparation. To account for these fluctuations, Benmouna *et al.*[6] refined the analogy to a dielectric by including a Debye-Hückel screening of the "charges," which permits long-range inhomogeneities leading to a nonvanishing zero-angle scattering. The screening length κ is determined self-consistently, by assuming that the scattering intensity at $k=0$ is not affected by the cross-linking as long as the temperature remains unchanged after preparation.[14] The free energy in the quadratic approximation then reads:

$$f(\{\Psi\}) = \tfrac{1}{2}{\sum_{\boldsymbol{k}}}'\left(\chi_{\mathrm{crit}} - \chi_m + k^2 + \frac{C}{k^2+\kappa^2}\right)\Psi_{\boldsymbol{k}}\Psi_{-\boldsymbol{k}}. \tag{72}$$

This expression can be compared with Eq. (51) in the quadratic approximation as follows:

$$f(\{\Psi\}) = \tfrac{1}{2}{\sum_{\boldsymbol{k}}}'\left(\frac{1}{\chi_m} - g_D(k^2) + \mu(\mu-1)\omega(k^2(\mu-1))\right)\Psi_{\boldsymbol{k}}\Psi_{-\boldsymbol{k}} \tag{73}$$

$$\approx \tfrac{1}{2}{\sum_{\boldsymbol{k}}}'\left(1 - \chi_m + k^2\frac{\chi_m}{3} + \mu(\mu-1)\omega(k^2(\mu-1))\right)\Psi_{\boldsymbol{k}}\Psi_{-\boldsymbol{k}}. \tag{74}$$

In the last line, we have expanded the Debye function for small wave number. We see that the microscopic model indeed agrees with phenomenological theories, provided we identify the phenomenological terms with the order parameter of the gel. The wave-number dependence of the order parameter is not Lorentzian; nevertheless, it decays monotonically with k, the relevant length scale being given by the localization length. Hence, the somewhat mysterious screening length is unambiguously identified with the localization length, which is computed self-consistently. Thereby, the microscopic model substantiates the picture of de Gennes and, furthermore, allows the computation of the parameters and functions that are beyond the phenomenological approach.

The frozen-in fluctuations were first addressed by Read *et al.*,[7] who considered a blend of polymer chains anchored at both ends to randomly chosen fixed points in space, in order to account approximately for the localization of chains due to the cross-links. Read *et al.* make reasonable but *ad hoc* assumptions about the distribution of the quenched random end-to-end vectors, and solve the resulting model within the random phase approximation. They obtain a scattering function that exhibits a nonzero value at $k=0$, due to the random, quenched fluctuations. In addition they compute the thermal, as well as the glassy, charge fluctuations as follows:

$$S_{\mathrm{var}}(k) = \frac{1}{\chi_{\mathrm{crit}} - \chi + k^2 + (C/k^2)} \quad \text{and} \tag{75}$$

$$S_{\mathrm{gl}}(k) = \frac{(C/k^2)^2|\rho_0(k)|^2}{(\chi_{\mathrm{crit}} - \chi + k^2 + (C/k^2))^2};$$

where $\rho_0(k)$ is the frozen-in concentration. The above results are in close correspondence to the results of our analysis, presented in Eqs. (32) and (34) and evaluated in the limit of small wave number as follow:

$$S_{\mathrm{var}}(k) \sim \frac{1}{1-\chi_m + k^2(\chi_m/3) + \chi_m(\mu-1)\omega(k^2/(\mu-1))},$$

$$S_{\mathrm{gl}}(k) \sim \frac{(\mu-1)w(k^2/(\mu-1))}{(1-\chi_m + k^2(\chi_m/3) + \chi_m(\mu-1)w(k^2/(\mu-1)))^2}.$$

Both approaches, the phenomenological one and the microscopic model, predict a divergence as microphase separation is approached, with the glassy correlations diverging twice as strongly as the thermal ones.

The work reported in the present paper can be extended in several directions. First, we have worked only on the level of mean-field and Gaussian fluctuations. It is known that the microphase separation transition in the symmetric case is rendered first order by fluctuations,[15] and hence it would be interesting to see the effect of fluctuations, even though the critical region is expected to be small.[16] Another extension is a cross-link probability that depends on the species. This would allow us to study, among other things, interpenetrating networks. Finally, it would be interesting to look at the dynamics of microphase separation.

ACKNOWLEDGMENTS

We thank Xiangjun Xing for enlightening discussions. This work was supported in part by the Deutsche Forschungsgemeinschaft through SFB 602 (AZ, CW), Grant No. Zi 209/6-1 (AZ), and GRK 782 (CW), and by the U.S. National Science Foundation through Grant No. NSF DMR02-05858, and the U.S. Department of Energy through Grant No. DEFG02-91ER45439 (PMG).

APPENDIX A: MICROPHASE MORPHOLOGY

To investigate microphase transition, we assume that the phase separation pattern can be described by a first-harmonic ansatz having a dominant wave number k and a definite lattice structure as follows:

$$\Psi_{\boldsymbol{k}'} = \Psi \frac{V}{\sqrt{2m}} \sum_{i=1}^{m} (\delta_{\boldsymbol{k}',+k\boldsymbol{n}_i} + \delta_{\boldsymbol{k}',-k\boldsymbol{n}_i}), \tag{A1}$$

with lattice vectors $n_i \in \mathbb{G} := \{\boldsymbol{n}_i | i=1,\ldots,m\}$ and an amplitude Ψ.

1. Lattice structures

We consider three particular morphologies, which are known to occur in the microphase separation of regular copolymer melts:[17,18]

(i) Lamellas ($m=1$): Alternating sheets rich in A and B; one-dimensional order. Lattice vector: $\boldsymbol{n}_1=(1,0,0)^T$.

(ii) Cylinders ($m=3$): Close-packed, i.e., hexagonally arranged, cylindrical domains, A in B or vice versa; two-dimensional order. Lattice vectors: $\boldsymbol{n}_1=(1,0,0)^T$, $\boldsymbol{n}_2=(-1/2,\sqrt{3}/2,0)^T$, and $\boldsymbol{n}_3=(-1/2,-\sqrt{3}/2,0)^T$.

(iii) bcc spheres ($m=6$): Spherical A-rich domains in B, or vice versa, on a bcc lattice in real space; three-dimensional order. Lattice vectors of the corresponding fcc lattice in Fourier space: $\boldsymbol{n}_1=(1,1,0)^T/\sqrt{2}$, $\boldsymbol{n}_2=(0,1,1)^T/\sqrt{2}$, $\boldsymbol{n}_3=(1,0,1)^T/\sqrt{2}$, $\boldsymbol{n}_4=(1,0,-1)^T/\sqrt{2}$, $\boldsymbol{n}_5=(-1,1,0)^T/\sqrt{2}$, and $\boldsymbol{n}_6=(0,-1,1)^T/\sqrt{2}$.

Note that $\boldsymbol{a} \in \mathbb{G} \Rightarrow -\boldsymbol{a} \notin \mathbb{G}$; therefore we introduce the symmetrized set of lattice vectors, $\mathbb{G}^+ := \{\boldsymbol{n} | \boldsymbol{n} \in \mathbb{G} \vee -\boldsymbol{n} \in \mathbb{G}\}$. For $m>1$, the set $\mathbb{G}$ of lattice vectors is not minimal in the sense of linear independence: for any two vectors $\boldsymbol{a} \neq \boldsymbol{b} \in \mathbb{G}$, the difference $\boldsymbol{a}-\boldsymbol{b}$ is included in $\mathbb{G}^+$. Rather, the vectors are chosen such that the $k_i \in \mathbb{G}^+$ point towards the directions of all nearest-neighbor lattice sites.

a. Wave-vector sums

Inserting the ansatz (A1) into the expansion of the Landau free energy of the random copolymer melt or the cross-linked homopolymer blend yields sums of the type

$$\begin{aligned}
&{\sum_{\boldsymbol{k}_{1,\ldots p}}}' f_2(\boldsymbol{k}_1,\ldots,\boldsymbol{k}_{p-1})\Psi_{\boldsymbol{k}_1}\cdots\Psi_{\boldsymbol{k}_p}\delta_{\Sigma_{\nu=1}^p \boldsymbol{k}_\nu,\boldsymbol{0}} \\
&= \frac{\Psi^p \cdot V^p}{(2m)^{p/2}} {\sum_{\boldsymbol{k}_{1,\ldots,p}}}' f_2(\boldsymbol{k}_1,\ldots,\boldsymbol{k}_{p-1}) \\
&\quad \times \prod_{\nu=1}^{p} \left(\sum_{\mu=1}^{m} (\delta_{\boldsymbol{k}_\nu,+k\boldsymbol{n}_\mu} + \delta_{\boldsymbol{k}_\nu,-k\boldsymbol{n}_\mu}) \right) \delta_{\Sigma_{\nu'=1}^p \boldsymbol{k}_{\nu'},0} \\
&= \Psi^p \cdot \frac{V^p}{(2m)^{p/2}} \sum_{\boldsymbol{k}_{1,\ldots,p} \in \mathbb{G}^+} f_2(\boldsymbol{k}_1,\ldots,\boldsymbol{k}_{p-1}) \delta_{\boldsymbol{k}_1+\cdots+\boldsymbol{k}_p,0}.
\end{aligned} \tag{A2}$$

In the quadratic sum the vertex function can be factored out, so that

$$\begin{aligned}
\frac{1}{V^2}\sum_{\boldsymbol{k}} f(k'^2)\Psi_{\boldsymbol{k}'}\Psi_{-\boldsymbol{k}'} &= \Psi^2 \cdot \frac{f(k^2)}{2m} \sum_{\boldsymbol{k}_{1,2} \in \mathbb{G}^+} \delta_{\boldsymbol{k}_1+\boldsymbol{k}_2,\boldsymbol{0}} \\
&= \Psi^2 \cdot f(k^2).
\end{aligned} \tag{A3}$$

The higher-order sums, however, strongly depend on the morphology of the microphases. In the simplest case, $f(\boldsymbol{k}_1,\ldots)=1$, the computation of these loops amounts to counting the number of closed loops that can be constructed with the vectors in $\mathbb{G}^+$. In general, the loops must also be classified with respect to their shape, i.e., planar or nonplanar, as distinct shapes yield distinct values of the vertex functions. The counting and classification have been done, e.g, in Ref. 18, with the results shown in Table I. For $f(\boldsymbol{k},\ldots)=1$, the third- and fourth-order sums are given by

$$\begin{aligned}
&\frac{1}{V^3}\sum_{\boldsymbol{k}_{1,2}} \Psi_{\boldsymbol{k}_1}\Psi_{\boldsymbol{k}_2}\Psi_{-\boldsymbol{k}_1-\boldsymbol{k}_2} \\
&= \Psi^3 \cdot \begin{cases} 0 & \text{for } m=1 \text{ (lamellas)} \\ \sqrt{2/3} & \text{for } m=3 \text{ (cylinders)} \\ 2/\sqrt{3} & \text{for } m=6 \text{ (bcc spheres)} \end{cases}
\end{aligned} \tag{A4}$$

and

TABLE I. Number of closed loops of p lattice vectors ("p loops") for different morphologies. The 4-loops are divided into intra- and extra-planar loops.

Loop type	Lamellas	Cylinders	bcc spheres
2-loop	2	6	12
3-loop	0	12	48
4-loop Planar	6	90	396
Nonplanar	⋯	⋯	144
Total	6	90	540

$$\frac{1}{V^4}\sum_{\boldsymbol{k}_{1,2,3}} \Psi_{\boldsymbol{k}_1}\Psi_{\boldsymbol{k}_2}\Psi_{\boldsymbol{k}_3}\Psi_{-\boldsymbol{k}_1-\boldsymbol{k}_2-\boldsymbol{k}_3} = \Psi^4 \cdot \begin{cases} 3/2 & \text{for } m=1 \text{ (lamellas)} \\ 5/2 & \text{for } m=3 \text{ (cylinders)} \\ 15/4 & \text{for } m=6 \text{ (bcc spheres)} \end{cases} . \tag{A5}$$

APPENDIX B: VERTEX FUNCTIONS

In the following, we define and compute the vertex functions appearing in the Landau expansion of the effective free energy, which are integrals over Wiener correlators of the type

$$\left\langle \exp\left\{ -i\sum_{\zeta=1}^{z} \hat{k}_\zeta \cdot \hat{r}(s_\zeta) \right\} \right\rangle_n^W = \delta_{\Sigma_{\zeta=1}^{s}\hat{k}_\zeta,0} \exp\left\{ \frac{1}{2}\sum_{\zeta,\zeta'} |s_\zeta - s_{\zeta'}| \hat{k}_\zeta \cdot \hat{k}_{\zeta'} \right\}; \tag{B1}$$

a derivation of Eq. (B1) can be found in Ref. 12. The correlator vanishes unless the wave vectors sum to zero in each replica. If just single-replica quantities are involved, the correlator factorizes,

$$\left\langle \exp\left\{ -i\sum_{\zeta_1=1}^{z_1} \boldsymbol{k}_{\zeta_1} \cdot \boldsymbol{r}^{\alpha_1}(s_{\zeta_1}) - \cdots - i\sum_{\zeta_m=1}^{z_m} \boldsymbol{k}_{\zeta_m} \cdot \boldsymbol{r}^{\alpha_m}(s_{\zeta_m}) \right\} \right\rangle_n^W = \left\langle \exp\left\{ -i\sum_{\zeta_1=1}^{z_1} \boldsymbol{k}_{\zeta_1} \cdot \boldsymbol{r}(s_{\zeta_1}) \right\} \right\rangle^W \cdots \left\langle \exp\left\{ -i\sum_{\zeta_m=1}^{z_m} \boldsymbol{k}_{\zeta_m} \boldsymbol{r}(s_{\zeta_m}) \right\} \right\rangle^W, \tag{B2}$$

for pairwise distinct $\alpha_1, \ldots, \alpha_m$, where $\langle \cdots \rangle^W$ denotes the unreplicated Wiener average.

1. Definition of the vertex functions

The second-order coefficients of the Landau expansion are governed by the *Debye function*

$$\begin{aligned} g_D(k^2) &:= \int_0^1 ds_1 ds_2 \langle e^{-i\boldsymbol{k}(\boldsymbol{r}(s_1)-\boldsymbol{r}(s_2))} \rangle^W \\ &= \int_0^1 ds_1 ds_2 \langle e^{-i\hat{k}(\hat{r}(s_1)-\hat{r}(s_2))} \rangle_n^W \\ &= \frac{e^{-k^2}-1+k^2}{k^4/2} \\ &= 1 - \frac{1}{3}k^2 + \frac{1}{12}k^4 + \mathcal{O}(k^6), \end{aligned} \tag{B3}$$

the scattering function for a noninteracting Gaussian chain.

The third-order correlators,

$$\begin{aligned} g_3(\boldsymbol{k}_1,\boldsymbol{k}_2) &:= \int_0^1 ds_1 ds_2 ds_3 \, \langle e^{-\Sigma_{\nu=1}^3 \boldsymbol{k}_\nu \boldsymbol{r}(s_\nu)} \rangle^W |_{\boldsymbol{k}_3=-\boldsymbol{k}_1-\boldsymbol{k}_2} \\ &= \int_0^1 ds_1 ds_2 ds_3 \, \langle e^{-i\Sigma_{\nu=1}^3 \hat{k}_\nu \hat{r}(s_\nu)} \rangle^W |_{\hat{k}_3=-\hat{k}_1-\hat{k}_2} \end{aligned} \tag{B4}$$

and

$$\begin{aligned} g_{\Psi^2\Omega}(\boldsymbol{k}_1,\boldsymbol{k}_2) &:= \int_0^1 ds_1 ds_2 ds_3 \langle e^{-i\boldsymbol{k}_1(\boldsymbol{r}(s_1)-\boldsymbol{r}(s_3))} \rangle^W \\ &\quad \times \langle e^{-i\boldsymbol{k}_2(\boldsymbol{r}(s_2)-\boldsymbol{r}(s_3))} \rangle^W \\ &= \int_0^1 ds_1 ds_2 ds_3 \\ &\quad \times \langle e^{-i\boldsymbol{k}_1 r^{\alpha_1}(s_1) - |\boldsymbol{k}_2 r^{\alpha_2}(s_2) - i\hat{k}\hat{r}(s_3)|} \rangle_n^W |_{\hat{k}=-\boldsymbol{k}_1\otimes e_{\alpha_1}-\boldsymbol{k}_2\otimes e_{\alpha_2}}^{\alpha_1\neq\alpha_2}, \end{aligned} \tag{B5}$$

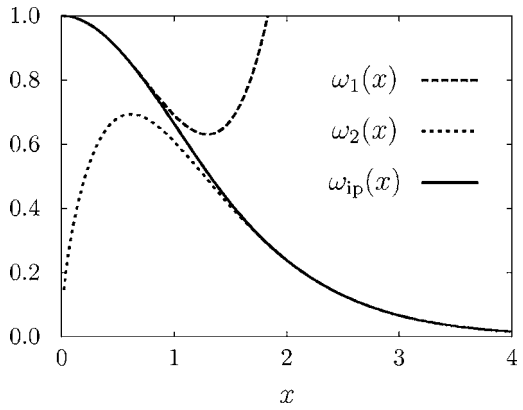

FIG. 11. Scaling function $\omega(x)$ vs x: Asymptotic expressions and interpolated function.

describe the correlation between three one-replica fields and the correlation between two one-replica fields and a higher-order replica field, respectively.

Finally, the fourth-order correlator is given by

$$g_{\Psi^4}(\boldsymbol{k}_1,\boldsymbol{k}_2,\boldsymbol{k}_3) = \int_0^1 ds_1 ds_2 ds_3 ds_4 \, \langle e^{-I\sum_{\nu=1}^4 \boldsymbol{k}_\nu \boldsymbol{r}(s_\nu)} \rangle^W |_{\boldsymbol{k}_4 = -\sum_{\nu=1}^3 \boldsymbol{k}_\nu}. \tag{B6}$$

a. Lamellar case

The third- and fourth-order correlators depend on the directions of the wave vectors. In particular, we require the "lamellar" case, in which all wave vectors are collinear. We note that $g_3(\boldsymbol{k},-\boldsymbol{k})=g_D(k^2)$, and define

$$\begin{aligned} g_3(k^2) &:= g_3(\boldsymbol{k},\boldsymbol{k}) \\ &= \frac{-(e^{-4k^2}-1+4k^2-8k^4)+64\left(e^{k^2}-1+k^2-\frac{1}{2}k^4\right)}{12k^6} \\ &\quad + \frac{2(e^{-k^2}-1+k^2)}{k^4} \\ &= 1-k^2+\frac{3}{4}k^4+\mathcal{O}(k^6), \end{aligned} \tag{B7}$$

$$\begin{aligned} g_{\Psi^2\Omega}(k^2) &:= g_{\Psi^2\Omega}(\boldsymbol{k},-\boldsymbol{k}) \\ &= \frac{-e^{-2k^2}+(8+2k^2)e^{-k^2}+4k^2-7}{k^6} \\ &= 1-\frac{2}{3}k^2+\frac{17}{60}k^4+\mathcal{O}(k^6), \end{aligned} \tag{B8}$$

and

$$g_{\Psi^4}(k^2) := g_{\Psi^4}(\boldsymbol{k},\boldsymbol{k},-\boldsymbol{k}) = \frac{144k^4-60k^2(9+4e^{-k^2})+784(1-e^{-k^2})-(1-e^{-4k^2})}{18k^8} = 1-\frac{2}{3}k^2+\frac{11}{30}k^4+\mathcal{O}(k^4). \tag{B9}$$

APPENDIX C: SCALING FUNCTION FOR THE GELATION ORDER PARAMETER

The localization lengths τ of monomers in the gel fraction of a cross-linked homopolymer melt or blend are distributed according to the distribution $p(\tau)$; see Sec. IV B. The fraction of the gel and the distribution are determined from the self-consistent solution of the saddle point equations with the order parameter hypothesis (20). The gelation order parameter, essentially the Laplace transform of $p(\tau)$, is proportional to a scaling function $\omega(x)$, which is computed in Ref. 12 in the asymptotic regimes of small and large x. For convenience, we define a rescaled version of ω,

$$w(k^2) := 2\cdot\omega(\sqrt{8k^2/3}). \tag{C1}$$

This also absorbs a factor of 2 arising from the different length scales used in Ref. 12 (the Wiener Hamiltonian used therein differs by a factor of 2).

1. Interpolation formula

The scaling function $\omega(k)$ defined in Ref. 12 can be described asymptotically by

$$\omega(x) \approx \begin{cases} \omega_1(x) := 1-0.4409x^2+0.1316x^4 & \text{for } x \ll 1, \\ \omega_2(x) := 3\left(\dfrac{\pi^2 x^6}{8\cdot 1.678}\right)^{1/4} e^{-\sqrt{2\cdot 1.678}x} \times \left(1+\dfrac{27}{40\sqrt{2\cdot 1.678}x}\right) & \text{for } x \gg 1, \end{cases} \tag{C2}$$

and is shown in Fig. 11. In order to access the whole range of $0<x<\infty$ we interpolate between the asymptotic regimes using the interpolation formula

$$\omega(x) \approx \begin{cases} \omega_1(x) & \text{for } x < \frac{1}{2}, \\ \omega_{ip}(x) & \text{for } \frac{1}{2} \leqslant x < 2, \\ \omega_2(x) & \text{for } x \geqslant 2, \end{cases} \tag{C3}$$

with the interpolating rational function

$$\omega_{ip} := \frac{b_0 + b_1 x}{1 + a_1 x + a_2 x^2 + a_3 x^3}. \tag{C4}$$

The coefficients $a_1 = -0.055$, $a_2 = 0.165$, $a_3 = 0.139$, $b_0 = 1.023$, and $b_1 = -0.194$ are chosen such that the value and first derivative of $\omega_{ip}(x)$ coincide with those of $\omega_1(x)$ at $x = 1/2$ and with those of $\omega_2(x)$ at $x = 2$; an additional sampling point is the numerical value $\omega(x = 1) = 0.664$.

APPENDIX D: FREE ENERGY OF THE FLUCTUATIONS ABOUT THE LAMELLAR STATE

In Sec. V we compute the Gaussian fluctuations about the lamellar state of a symmetric, incompressible gel. This requires the quadratic expansion of the effective free energy, which is indicated in Eq. (66) in a compact form. In full detail the expansion reads

$$\begin{aligned}
\frac{n}{N}\mathcal{F}_n(\{\Phi\}) \approx{}& \tfrac{1}{2}\sum_{\alpha_{1,2}}\sum_{\boldsymbol{p}}{}' A_{\alpha_1\alpha_2}(p)\Phi_{\boldsymbol{p}}^{\alpha_1}\Phi_{-\boldsymbol{p}}^{\alpha_2} + \psi^2\cdot\sum_{\alpha>0}\sum_{\boldsymbol{p}}{}'\left(g_D(k^2)g_D(p^2) + \frac{2(g_3(\boldsymbol{k},\boldsymbol{p}))^2}{g_D((\boldsymbol{k}+\boldsymbol{p})^2)} - g_{\Psi^4}(\boldsymbol{k},-\boldsymbol{k},\boldsymbol{p})\right)\Phi_{\boldsymbol{p}}^{\alpha}\Phi_{-\boldsymbol{p}}^{\alpha} \\
&+ \tfrac{1}{2}\psi^2\cdot\sum_{\alpha>0}\sum_{\boldsymbol{p}_{1,2}}{}'\delta_{\boldsymbol{p}_1+\boldsymbol{p}_2+2\boldsymbol{k},\boldsymbol{0}}\left(\frac{g_3(\boldsymbol{k},\boldsymbol{k})g_3(\boldsymbol{p}_1,\boldsymbol{p}_2)}{g_D(4k^2)} + \frac{2g_3(\boldsymbol{k},\boldsymbol{p}_1)g_3(\boldsymbol{k},\boldsymbol{p}_2)}{g_D((\boldsymbol{k}+\boldsymbol{p}_1)^2)} - g_{\Psi^4}(\boldsymbol{k},\boldsymbol{k},\boldsymbol{p}_1)\right)\Phi_{\boldsymbol{p}_1}^{\alpha}\Phi_{\boldsymbol{p}_2}^{\alpha} \\
&+ \tfrac{1}{2}\psi^2\cdot\sum_{\alpha>0}\sum_{\boldsymbol{p}_{1,2}}{}'\delta_{\boldsymbol{p}_1+\boldsymbol{p}_2-2\boldsymbol{k},\boldsymbol{0}}\left(\frac{g_3(\boldsymbol{k},\boldsymbol{k})g_3(\boldsymbol{p}_1,\boldsymbol{p}_2)}{g_D(4k^2)} + \frac{2g_3(\boldsymbol{k},-\boldsymbol{p}_1)g_3(\boldsymbol{k},-\boldsymbol{p}_2)}{g_D((\boldsymbol{k}-\boldsymbol{p}_1)^2)} - g_{\Psi^4}(\boldsymbol{k},\boldsymbol{k},-\boldsymbol{p}_1)\right)\Phi_{\boldsymbol{p}_1}^{\alpha},\Phi_{\boldsymbol{p}_2}^{\alpha},
\end{aligned} \tag{D1}$$

with $A_{\alpha_1,\alpha_2}(p)$ denoting the quadratic vertex function of the homogeneous gel defined in Eq. (23) and with the saddle point amplitude ψ and wave vector $\mathbf{k}$ of the lamellar microphases.

[1] R. T. Deam and S. F. Edwards, Philos. Trans. R. Soc. London, Ser. A **280**, 317 (1976).
[2] P. G. de Gennes, J. Phys. (France) Lett. **40**, L-69 (1979).
[3] R. M. Briber and B. J. Bauer, Macromolecules **21**, 3296 (1988).
[4] H. Jinnai, H. Hasegawa, T. Hashimoto, R. M. Briber, and C. C. Han, Macromolecules **26**, 182 (1993).
[5] A. Bettachy, A. Derouiche, M. Benhamou, and M. Daoud, J. Phys. I **1**, 153 (1991).
[6] M. Benmouna, T. A. Vilgis, M. Daoud, and M. Benhamou, Macromolecules **27**, 1172 (1994).
[7] D. J. Read, M. G. Brereton, and T. C. B. McLeish, J. Phys. II **5**, 1679 (1995).
[8] S. Panyukov and Y. Rabin, Phys. Rep. **269**, 1 (1996).
[9] C. D. Sfatos and E. I. Shakhnovich, Phys. Rep. **288**, 77 (1997).
[10] S. Lay, J.-U. Sommer, and A. Blumen, J. Chem. Phys. **113**, 11355 (2000).
[11] C. Wald, A. Zippelius, and P. M. Goldbart, Europhys. Lett. **70**, 843 (2005).
[12] P. M. Goldbart, H. E. Castillo, and A. Zippelius, Adv. Phys. **45**, 393 (1996).
[13] S. Alexander and J. McTague, Phys. Rev. Lett. **41**, 702 (1978).
[14] A. Bettachy, A. Derouiche, and M. Benhamou, Macromol. Theory Simul. **4**, 67 (1995).
[15] S. A. Brazovskiĭ, Zh. Eksp. Teor. Fiz. **68**, 175 (1975) [Sov. Phys. JETP **41**, 85 (1975)].
[16] M. Benhamou, A. Derouiche, and A. Bettachy, J. Chem. Phys. **106**, 2513 (1996).
[17] L. Leibler, Macromolecules **13**, 1602 (1980).
[18] A. M. Mayes and M. Olvera de la Cruz, J. Chem. Phys. **91**, 7228 (1989).